Politecnico di Torino

Politecnico di Torino

Master's Degree in Biomedical Engineering
A.Y. 2022/2023

Master's thesis

Tailoring of polymeric carbon dots by using organic dyes for radical scavenging

Supervisors:
Prof. Alberto Tagliaferro
Dr. Mattia Bartoli

Candidate:
Francesco Rapisarda

July 2023

ABSTRACT

Carbon dots (CDs) are emerging as versatile fluorescent nanomaterials due to their excellent properties such as high-water solubility, photostability, good biocompatibility, flexibility for surface modification, low toxicity and production costs. These characteristics make them preferable to their inorganic cousins Quantum Dots and more suitable for biomedical applications, such as imaging, antibacterial therapy, drug delivery for cancer treatment, photodynamic therapy and antioxidative nanotechnology. Regarding the last field, CDs have proven to possess scavenging activity towards Reactive Oxygen Species (ROS), which are chemical, highly reactive, oxygen-containing species including hydroxyl radical ($OH\bullet$), singlet oxygen ($^1O_2$), superoxide anion ($O_2\bullet-$), and hydrogen peroxide (H_2O_2). This antioxidant capability allows CDs to act as effective agents capable of keeping the concentration of ROS low, preventing various diseases such as cancer, atherosclerosis, neurological disorders, asthma, hypertensions, local anaphylaxis or inflammation. In this thesis work, three different types of CDs were synthetized by ultrasonic-assisted method using Citric Acid (CA) and p-Phenylendiamine (p-DPA) as precursors. First of all, pristine CDs with only CA and p-DPA as reagents were synthesized. Then, two organic dyes, Methylene Blue and Cochineal Red were added keeping the other two precursors and the synthesis method unchanged, in order to create more performant CDs (second and third type respectively) for what concern scavenging activity and red-shifted fluorescence emission, resulting in less energy been released and making them hopefully more suitable for biomedical field.

All CDs were characterized through different spectroscopic techniques in order to investigate structural and photophysical properties of the three types of CDs obtained.

Lastly, solutions of CDs and another organic dye (Curcumin) were prepared in order to investigate and evaluate CDs scavenging activity.

CONTENTS

CHAPTER 1 INTRODUCTION

1.1 Reactive Oxygen Species (ROS): an overview

Reactive oxygen species (ROS) are chemical, highly reactive, oxygen-containing species including hydroxyl radical (OH•), singlet oxygen ($^1O_2$), superoxide anion ($O_2^{\bullet -}$), and hydrogen peroxide (H_2O_2) [1]. ROS are involved in important physiological processes such as thyroid hormone production and crosslinking of extracellular matrix and work as regulatory mediators in various signalling pathways, such as cell proliferation, activation and migration [1], [2]. They are also involved in degradation of chemical products and polymers and food spoilage [3]–[5]. Most of the ROS are by-products from mitochondrial electron transport chain in organisms, a fundamental mechanism for cellular respiration, corresponding to the first part of oxidative phosphorylation [6]. Under normal physiological conditions, ROS are generated in controlled ways and maintained at low concentrations, as they can be eliminated through protective mechanisms including enzymatic or nonenzymatic antioxidants.

Problems emerge when dealing with high amounts of ROS, due to an increased ROS production (whose cause may be normal biochemical reactions, excessive exposure to UV radiation, long-term stress conditions, intense physical exercise, higher level of xenobiotics[7], [8]) and/or a decreased ROS scavenging activity, which can provoke oxidative stress. The latter could induce multiple changes in physiological process and can result in irreparable damages to molecular and cellular structures like carbohydrates, proteins, nucleic acids (both DNA and RNA) and lipids leading to numerous diseases such as cancer [9], atherosclerosis [9], neurological disorders [10], asthma [11], hypertensions [12], local anaphylaxis [13] or inflammation [13].

1.1.1 Radical scavenging activity of main natural enzymatic and nonenzymatic antioxidants and emerging problems

Focusing on radical scavenging activities of main antioxidants, we will start discussing natural enzymatic ones which comprise superoxide dismutase (SOD), glutathione peroxidase (GSHPx) and catalase (CAT).

SOD is located in the cytosol and mitochondria and, in presence of metal ion cofactors such as copper (Cu), zinc (Zn) or manganese (Mn), catalytically convert the $O_2^{\bullet -}$ into ordinary molecular oxygen and hydrogen peroxide, which are two less damaging species, according to this reaction mechanism:

$$2\,H^+ + 2\,O_2^{\bullet -} \xrightarrow{(SOD)} O_2 + H_2O_2 \qquad [7]$$

Glutathione peroxidase is found both in the cytoplasm and at the extracellular level in almost all human tissues and converts the hydrogen peroxide into the water thanks the aid of glutathione (GSH) which is transformed in glutathione disulfide (GSSG), according to this reaction:

$$H_2O_2 + GSH \xrightarrow{(GSHPx)} GSSG + H_2O \qquad [7]$$

The last one, Catalase, which is a haem protein, converts hydrogen peroxide into water and molecular oxygen as follows:

$$2\,H_2O_2 \xrightarrow{(CAT)} 2\,H_2O + O_2 \qquad [14]$$

There are also nonenzymatic antioxidants which can be divided into two categories: natural and synthetic antioxidants. Among the first, Vitamin E (α-tocopherol) is an efficient lipid soluble antioxidant, found in vegetables, that functions as a 'chain breaker' during lipid peroxidation in cell membranes.

It intercepts lipid peroxyl radicals ($LOO^{\bullet}$) resulting in the formation of a relatively stable and insufficiently reactive tocopheroxyl radical, according to this reaction mechanism:

$$LOO^{\bullet} + \alpha\text{-tocopherol-OH} \longrightarrow LOOH + \alpha\text{-tocopherol-O}^{\bullet} \qquad [7]$$

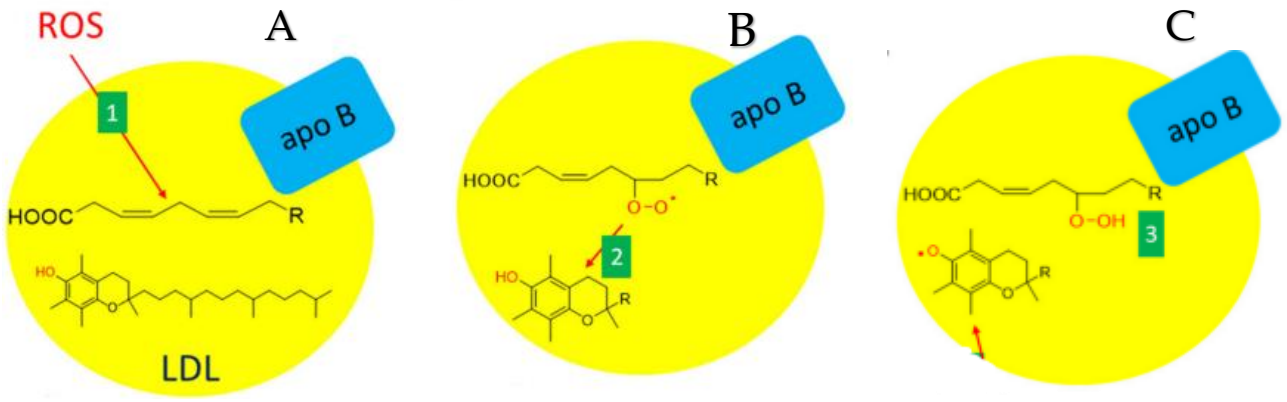

Figure 1. A) Unsaturated fatty acid within the LDL (low-density lipoprotein) particle is oxidized (f or example, by other ROS) and a lipid peroxyl radicals is formed. B-C) Then, the latter is intercepted by Vitamin E (α-tocopherol) resulting in the formation of a lipid hydroperoxide and tocopheroxyl radical. (Adapted with permission from source [15]).

Another example of natural nonenzymatic antioxidants is given by Vitamin C, called also ascorbic acid ($AscH_2$), which is an essential micronutrient for human health, acquired mainly through citrus fruits, such as lemon and orange, and vegetables. It can be found in its deprotonated form ASCH- (ascorbate), and react with a radical, generally a lipid radical by donating an electron to the latter and stop the lipid peroxidation chain reaction, giving rise to a more stable and less reactive radical called ascorbyl free radical. The reaction mechanism is illustrated below:

Figure 2. Reaction mechanism of antioxidant activity of Vitamin C. (Adapted with permission from source [16].

The last reported example concerning natural nonenzymatic antioxidants is Curcumin. As it is known from literature, Curcumin, which is a natural polyphenolic spice obtained from the tropical southeast Asian plant Curcuma Longa (turmeric), it is considered as a good dietary supplement for its anti-inflammatory, analgesic, antiseptic properties [9]. Li et al. demonstrated also its therapeutic effect against cancer cells, which may be improved by developing a highly water-soluble nano-formulation consisting in Curcumin micelles [17]. Furthermore, Curcumin itself has shown to have antioxidant and radical scavenging properties, and, in particular, it is commonly believed that the latter depends on H abstraction from one of its phenolic hydroxyl groups, although there are other theories that consider CH2 in the centre of the molecule's skeleton to be the leading site for the reaction with the radical.

Below is a diagram made by Nimse & Pal, depicting the reaction mechanism of curcumin with formation, after numerous steps, of the final product bicyclopentadione [7].

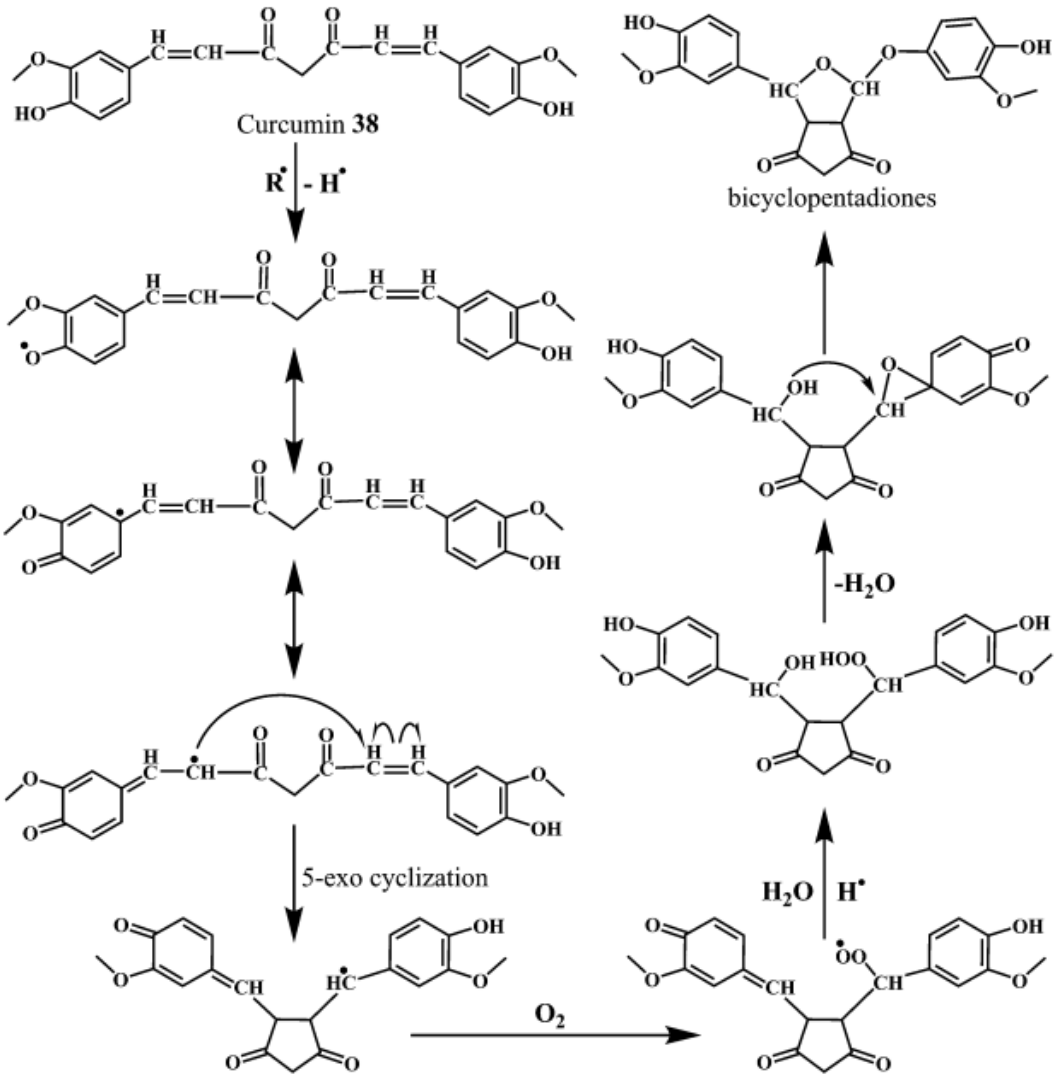

Figure 3. Mechanism of radical scavenging activity of curcumin 38 initiated by phenolic moiety. (Reproduced with permission from source [7]).

It also proved to be capable of upregulating HO-1 and γ-GCS antioxidant genes [18]. On the other hand, Curcumin suffers from certain weaknesses, like low water solubility, rapid degradation, and fast metabolism.

1.1.2 Radical scavenging activity of main synthetic nonenxymatic antioxidants and emerging problems

Previously discussed natural antioxidants, mainly enzymatic ones, are usually unstable, not cost-effective, sensitive to physiological conditions and insufficient in ROS scavenging [19]–[21].

An alternative solution for radical scavenging and regulation of ROS concentration is given by synthetic nonenzymatic antioxidants, and, in particular, by synthetic phenolic antioxidants (SPA), characterized by phenolic rings substituted by hindered alkyls in the ortho position. A representative synthetic phenolic antioxidant is 2,6-di-tert-butylhydroxytotulene (BHT), which is widely used in mineral oil, food, polymer, drug, cosmetic and other fields [21]. The cause of its antioxidant capability has to be found in its chemical structure: in fact, electron-donating alkyl groups on the ortho and para positions of BHT increase the electron density of the phenolic hydroxyl moiety through the inductive effect and the hyperconjugation effect, reduce the bond dissociation energy of the phenolic hydroxyl group, and enhance its reactivity to lipid free radicals, allowing it to easily yield a hydrogen atom to the last ones. Below, other two different reaction mechanisms of BHT with OH•, proposed by Zhou et al., are shown. First one, refers to a H-atom abstraction from the t-butyl group leading to the formation of isobutene, while the second represents an addition reaction to aromatic ring by the radical at C2 site of BHT, with the formation of a tertiary butyl.

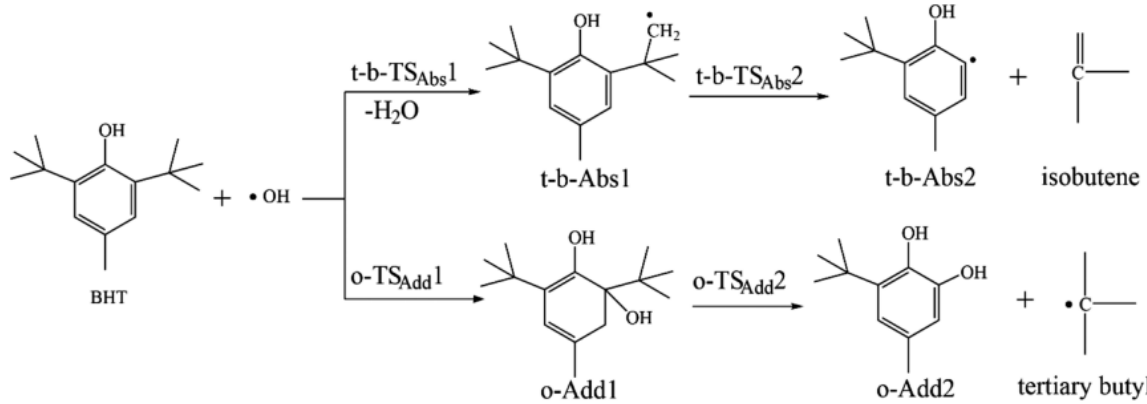

Figure 4. Proposed mechanism of reaction between BHT and OH•. (Reproduced with permission from source [21]).

Phenolic ring is also found in another SPA antioxidant, butylated hydroxyanisole (BHA), and for this reason, the latter shares with BHT the mechanism of reaction with ROS. BHA is used for the preservation of soybean and palm oil in cereal and confectionery products [22].

Even if their antioxidant activity is well established, previous studies have found that some SPAs showed toxicity effects and may cause liver damage and carcinogenesis [23]–[25]. This makes it necessary to turn our attention to other solutions, also considering the limits of natural antioxidants that were previously discussed. Various nanomaterials have been shown antioxidant activities and, among these, Carbon Dots (CDs) have recently attracted much attention, also considering their other applications such as biological sensors, antibacterial agents, photodetectors, drug delivery systems for cancer cell treatment [13], [26]–[35].

1.2 Carbon Dots (CDs)

1.2.1 An ovierview

CDs are zero-dimensional (0D) carbon nanomaterials, structurally consisting of cores with sp^2 conjugated carbon surrounded by amorphous shells with many surface functionalities, such as carboxyl, amine, hydroxyl and carbonyl moieties [19], discovered by fortuitous chance by Xu et al. during a purification process of multiwalled-CNTs.

CDs are emerging as versatile fluorescent nanomaterials thanks to their excellent properties, such as high water solubility and flexibility for surface modification (due to the presence of the previous mentioned polar moieties) [36], [37], photostability, tunable excitation and emission wavelengths, good biocompatibility, low toxicity, and thanks to their ability to mimic the structures and functions of natural enzymes [19], [29], [38]–[41]. Another characteristics of CDs which lead them to have low costs of production compared to other nanoparticles, is that they can be obtained from biomass, such as waste tea [42] and food scraps [43], orange peel and lemon peels [44], coffee [45], tobacco leaves [46] and garlic [47].

These characteristics make them preferable to their inorganic cousins Quantum Dots (QDs) and more suitable for the biomedical applications mentioned before [36]. Among these, phototheranostics represents a very important field with a lot of potential, combining diagnosis and image-guided therapy for some diseases like cancer. To date, most research has focused on using two separate 'players' to combine imaging and therapy, for example by exploiting fluorescent agents to detect and monitor the tumour before, after and during treatment, and photosensitisers stimulated by light irradiation for the generation of ROS responsible for treating the tumour itself. Over time, there has been a shift towards the employment of certain photosensitisers capable of combining both functions. For this purpose, organic compounds such as phthalocyanine, porphyrin and bacteriochlorin have been used, but these have shown limitations as they exhibit excitation and emitting wavelengths in general in the UV/VIS region, so that the performance of fluorescence imaging and phototherapy are both disadvantaged due to the poor tissue penetration power of this particular wavelength range, far from the conventional phototherapeutic window (700-900 nm) [48]. Other traditional PSs suffer from certain disadvantages like low water solubility and high oxygen dependency [6] where the tumour microenvironment is instead characterised by low oxygen availability and reduced partial oxygen pressure [28], [35].

Other attempts have been made to combine PDT with other types of phototherapy such as photothermal therapy (PTT), using one agent for PDT (e.g., carbon nanomaterials) and another for PTT (e.g., gold nanoparticles) for better therapeutic efficiency. However, this approach has other disadvantages such as the need to use two lasers with two different wavelength ranges to simultaneously excite PSs (with visible light) and PTT agents (with near infrared laser). All these disadvantages regarding phototherapeutic approaches can be overcome, at least in part, by CDs.

Additionally, CDs have been shown to be excellent antioxidants, which will be the main focus of this thesis work.

In order to improve the abovementioned shortcomings of Curcumin (**section 1.1.1**), many efforts were made in implementing appropriate nanocarriers, in the wake of what Li et al. did (see **section 1.1.1**).

Arvapalli et al were among the first to recognise the ability of CDs to act as nanocarriers and tried to combine the characteristics and advantages of CDs and Curcumin itself. For this purpose, they prepared a particular type of CD with Curcumin ethylenediamine and citric acid as precursors, giving rise to potential efficient candidates for bioimaging and antioxidant therapy [9].

In this thesis work, one of our aims will be to demonstrate that CDs prepared are able to protect Curcumin and prevent it from degrading, imagining a possible therapeutic approach by which CDs could be used as carriers to transport Curcumin to certain locations, so that it performs its antioxidant function efficiently, preventing it from being degraded before reaching the desired site in the human body.

The antioxidant activity of CDs generally results from their abundant reductive functional groups.

Before addressing the antioxidant/radical scavenging capacity of CDs, an in-depth examination of CDs structure and classification will be made, and their most important properties will be discussed.

1.2.2 Classification of Carbon Dots

A first CD classification is merely production-based and includes two categories: top–down and bottom–up methods. Top–down methods consist of the cutting of carbon materials into carbon nanoparticles, and comprise laser ablation, arc discharge, electrochemical route and plasma treatment. Bottom-up methods consist in obtaining CDs from molecules or polymers precursors, which, during the synthesis, go through carbonization and dehydration processes. These include, among others, hydrothermal and solvothermal methods, microwave-assisted methods, ultrasonic-assisted methods, combustion, chemical vapor deposition. CDs prepared through bottom-up methods usually don't have a clear distinction between the core and shell as those obtained by top-down approaches [49]. Both approaches require further purification steps in order to isolate the nanoparticles generally performed through dialysis or chromatography [50], [51]. In the figure below, main pros and cons of both methods can be noticed.

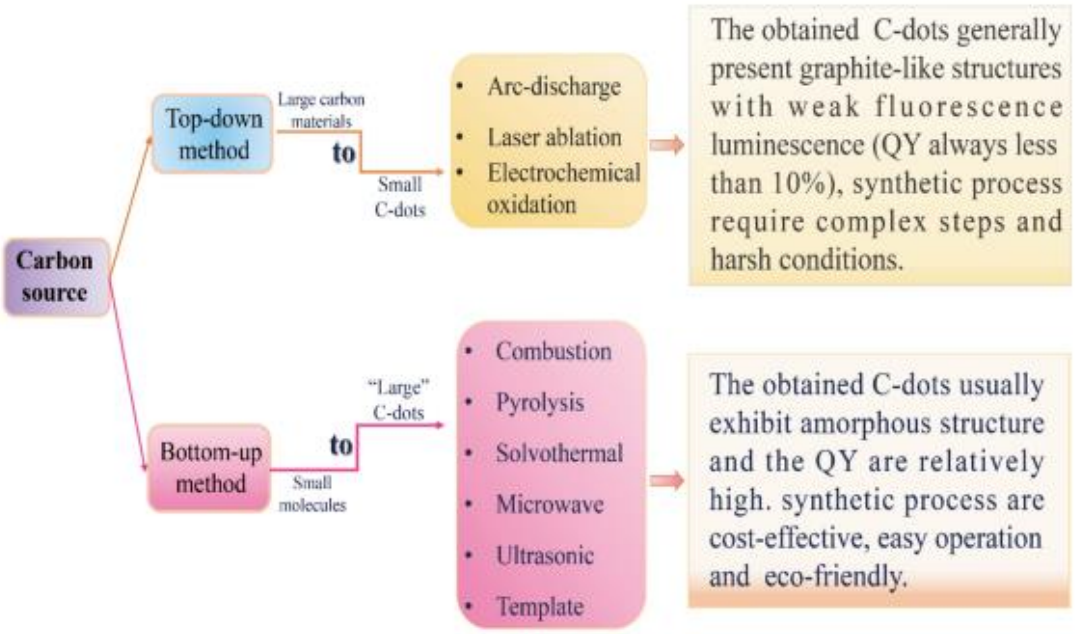

Figure 5. Top-down and bottom-up approaches for CDs synthesis. (Reproduced with permission, source [52]).

Another classification is based on their structure and chemical features. Considering core and shell organization and Hia et al. valuations, we can distinguish 4 classes of CDs:

I. Graphene Quantum Dots (GQDs)
II. Carbon Quantum Dots (CQDs)
III. Carbon Nanodots (CNDs)
IV. Carbon Polymeric Dots (CPDs)

GQDs possess a core of one or a few π-conjugated parallel graphene layers (usually less than five [49]) and connected chemical groups on the edges and could have circular shape with a thin thickness compared to their width [53]. The CQDs are always spherical and possess clear crystal lattices and chemical groups on the surface, instead of CNDs which usually show non-evident crystal lattices structure and polymer features and which have a high carbonization degree with some chemical groups on the surface such as nitrogen. [49]. CPDs possess a polymer/carbon hybrid structure containing a carbon core and abundant functional groups/polymer chains on the surface. The carbon core can be divided in 4 classes: two types of fully carbonised cores similar to the CNDs or CQDs [54], a paracrystalline carbon structure composed of tiny carbon clusters surrounded by polymer frames [54], [55], and a highly dehydrated cross-linking with close-knit polymer frame structure [56], [57].

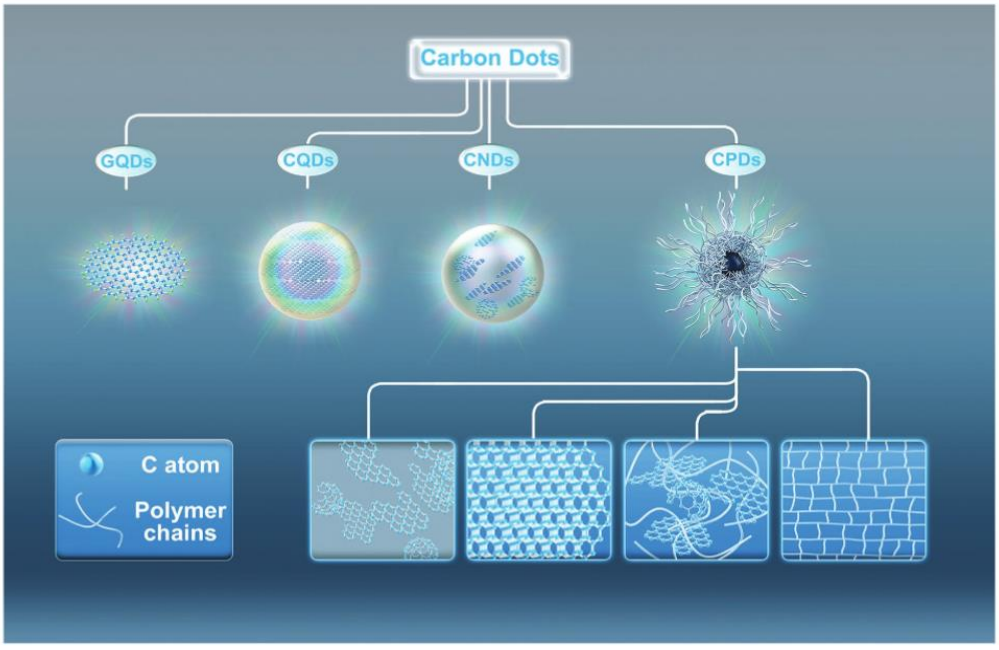

Figure 6. Classification of CDs, including the possible structures of carbon core of CPDs. (Reproduced with permission, source [49]).

1.2.3 Optical properties

CDs typically show strong optical absorption in the UV region (230–320 nm), with a tail extending into the visible range. For the carbon core, a maximum peak at ≈ 230-260 nm is ascribed to the π–π^* transition of aromatic C=C bonds, while another shoulder at ≈ 300-350 nm is attributed to the n–π^* transition of C=O bonds or other connected groups with lone pairs electron.

Regarding photoluminescence properties, the most common CDs have strong PL from blue to green, and a few CDs possess optimal emission in long-wavelength regions [58]–[60]. The emission peaks of CDs are usually wide, with large Stokes shifts compared to the emission of organic dyes and QD. This wide peak may result from the inhomogeneous chemical structure and diverse PL centres, as will be seen later. The emission peak position is generally related to the excitation wavelength, which is known as wavelength-dependent behaviour.

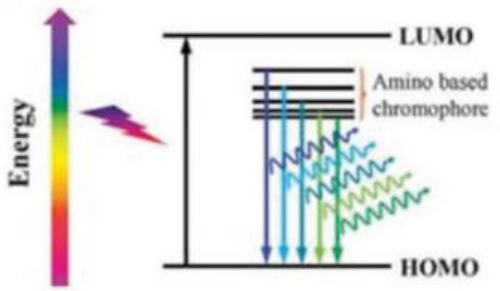

Figure 7. Illustration of excitation-dependent behaviour of CPDs. (Reproduced with permission, source [61]).

There are a lot of works in literature which tried to identify and explain the main factors governing the photoluminescence (PL) properties of CDs. Based on some studies ([36], [52], [53], [62], [63] it's possible to list the most relevant ones as follows:

I. *π-conjugated domains present in the core;*

II. *Quantum size/confinement effect;*

III. *Surface states related to chemical composition, functional groups of the particle's shell and surface defects;*

IV. *The cross-linked enhanced emission effect (CEE).*

V. *Molecule state related to the presence of fluorophores produced during the CDs formation, which are located at the outer or inner space of the particles.*

VI. *The parameters of synthesis reactions.*

When an incident radiation strikes a fluorescent substance, it excites its atoms, promoting an electron to a less bound more energetic and thus more 'outer' level. Within a few tens of nanoseconds, the excited electron returns to its previous level in two or more stages, passing through one or more excited states at intermediate energy.

A core of a CD usually contains sp^2 -hybridized domains immersed in an amorphous sp^3 -hybridized matrix. With a diffuse electron cloud over a large part of their core due *to π-system of sp^2 domains (I)*, CDs are easily and highly affected by the fluorescence phenomenon. A GQD with fewer surface chemical groups and a perfect graphene core would have a photoluminescent centre in the band gap of the conjugated π-domain. CDs that possess an extended π systems (such as GQDs) can be modified through π interaction with small aromatic molecules. This extends conjugation domains leading to reduction of HOMO-LUMO gap and red-shifted fluorescence [64], also resulting in an increase in quantum yield, photostability, and biocompatibility [36],[65].

CDs usually have a particle size of less than 10 nm, and therefore exhibit '*quantum size/confinement effect*' *(II),* the second PL-determining factor of the previous list. It occurs when carbon dots are smaller than their exciton Bohr radius. When the particle size of C-dots increases, their maximal fluorescent emission wavelengths show a red-shift. Some works suggested that quantum yield (QY) can be improved by reducing the size of CDs which causes an increase of the HOMO-LUMO gap and enhances the abovementioned property [53].

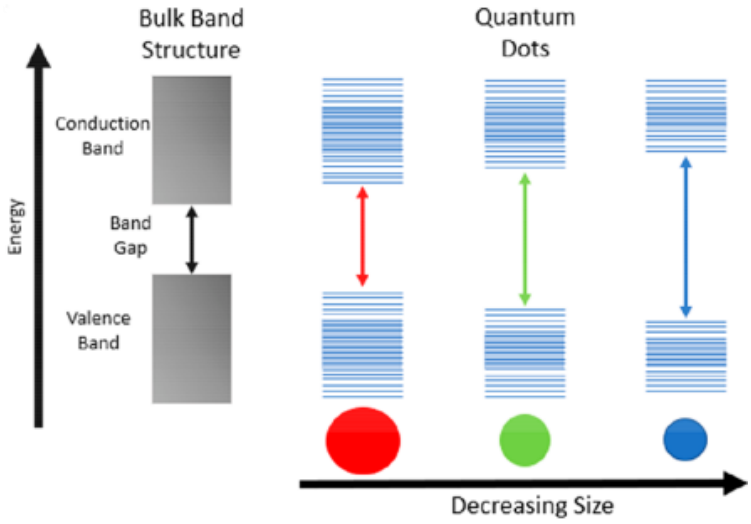

Figure 8. Schematic representation of 'quantum size/confinement effect'. (Reproduced with permission, source [36].

Unlike QDs, particle size does not seem to play a relevant role in the regulation of fluorescence compared to the presence of certain functional groups on the surface, which, together with other factors which will be investigated later, merge into what is known as '*surface state' (III*) [53]. In fact, as reported by previous studies, it's possible to tune the emissions of CDs by introducing an upward shift in the Fermi level and electrons in the conduction band [36],[66]. A way to achieve this is doping with heteroatoms. The latter could be added as doping agents after the synthesis or could be integrated into the graphene-like structure during the production of CDs as in the case of CQDs and CNDs.

An example is the doping of CDs with an heteroatom like nitrogen, the most common dopant used to change the fluorescent properties of CD due to its 5 valence electrons and similar size to carbon [36][67].

Generally, heteroatom doping is an effective way to improve optical properties of CDs, including the enhancement in fluorescence intensity and redshift of emission wavelength. In particular, the latter effect is due to their ability in regulating the initial band gap and forming new energy levels between HOMO (highest occupied molecular orbital) and LUMO (lowest unoccupied molecular orbital).

On the contrary, other works affirm that doping CDs with high electronegative atoms, such as nitrogen, causes a blue-shifted emission [68]. This is confirmed by Du et al. studies which suggest that amides play a major role in the blue emission while low electronegative atoms doping, such as phosphorus and boron, lead to a red-shifted emission [66]. Instead, it is commonly believed that redshifted emission can be obtained with the introduction of carboxylic derivatives and other oxygen containing functional groups [69]–[73]. These, according to Tetsuka et al. are also responsible for the decreasing of QY, as they act as non-radiative electron-hole recombination centres, and this is confirmed by Zheng et al. and Eda et al. [74]–[76].

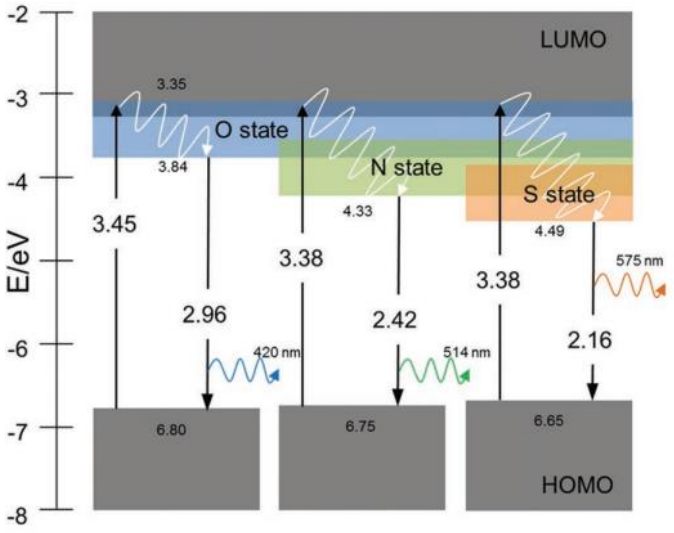

Figure 9. Schematic representation of the energy level structure of CPDs with non-doping, nitrogen doping, and sulphur doping. (Reproduced with permission, source [77]).

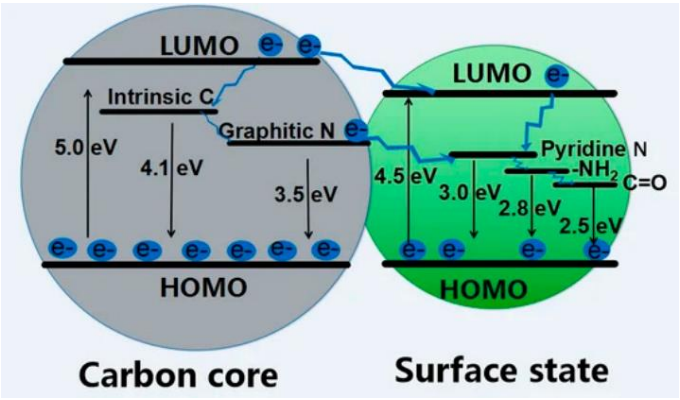

Figure 10. Scheme of the fluorescence emission of CDs based on different core/shell size ratios. (Reproduced with permission, source [78]).

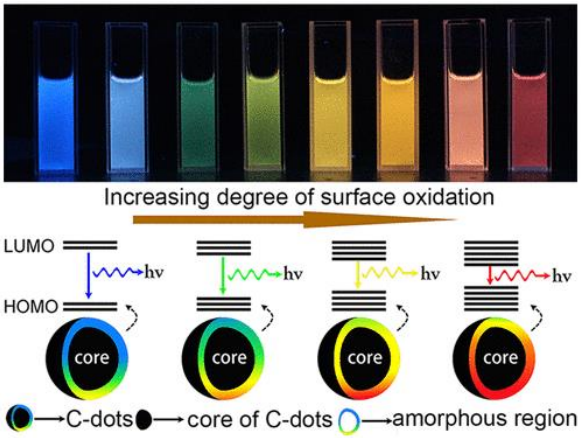

Figure 11. Influence of surface oxidation degree on PL. (Reproduced with permission, source [73]).

Surface passivation and some other treatments enriching the surfaces of CDs with amino, hydroxyl and carboxyl functional groups can improve the water solubility of CDs and make it easier to functionalise the surface, which can lead to plenty of application of CDs [52]. Surface passivation includes two major approaches: insertion in the structure of CDs some long-chain agents and surfaces oxidation with strong acids [52]. Due to the usual presence of long-chain carboxylic acids and some other functional substances in carbon sources, carbonization and passivation occur at the same time during the synthetic process of CDs from biomass waste [52]. As a result, CDs synthesized from biomass waste are often self-passivated and therefore, generally exhibit good optical properties [52].

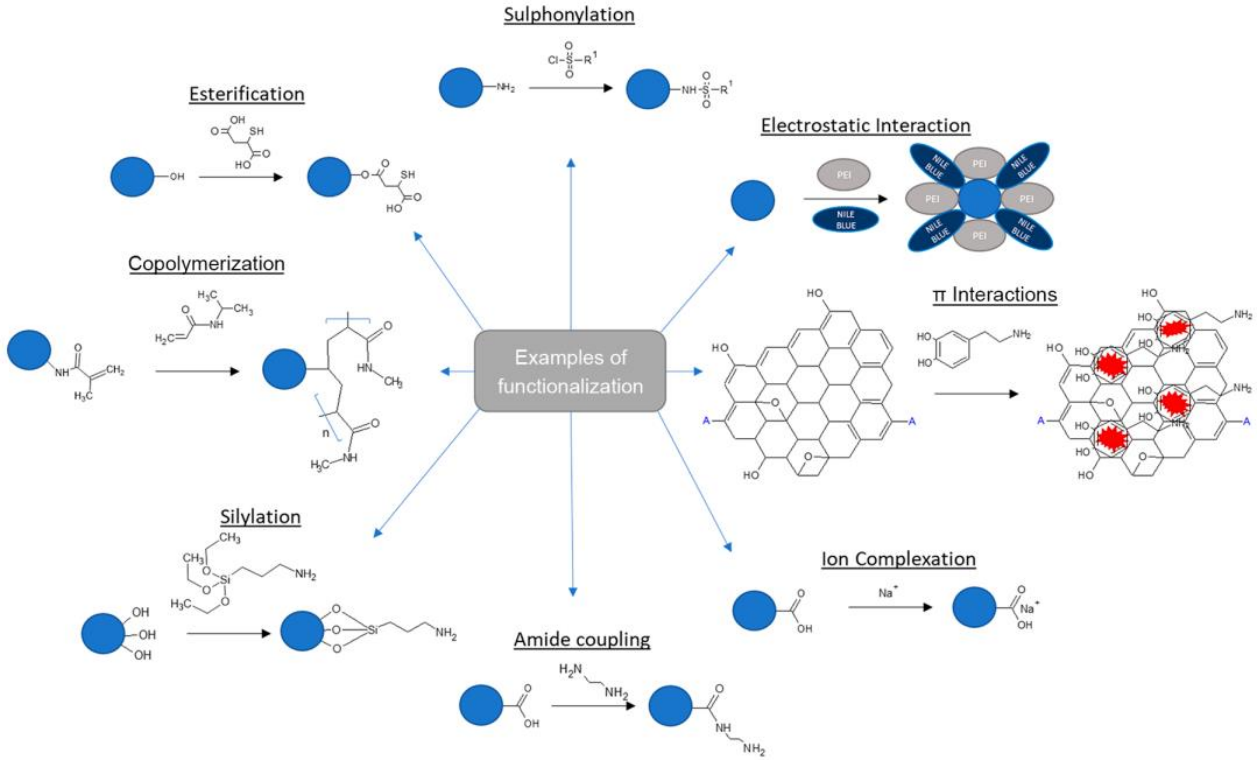

Figure 12. Examples of covalent and noncovalent modification to CDs. (Reproduced with permission, source [36]).

Still concerning the third point of the previous list, another fluorescence mechanism in CDs is the fluorescence originated from the *defects* [36],[79]. The defect site refers to the sites that miss having a perfect sp2 domain. The non-perfect sites cause surface energy traps that can act as capture centers for excitons, thus giving rise to surface defect state-related fluorescence [63], [80]. Furthermore, if the CDs are functionalized or surface passivated, this results in more stabilization of the surface defects which in turn leads to facile radiative recombination of the electron/hole pairs, confined on the surface [36],[79].

As regards the *CEE (IV),* this phenomenon was firstly described by Tao et al. [57] by comparing the fluorescence emission of poly(ethylenimine) with CPDs-derived materials produced by the degradation and crosslinking of the polymer. The authors reported an increase of fluorescence emission and they suggested that this was due to the formation of a rigid structure able to forbid the intramolecular rotations and vibrations promoting the fluorescence emission. This was supported by other studies, indicating that the mobility reduction of the covalent bond due to steric hindrance or supramolecular interactions may contribute to reduce the nonradiative relaxation and to improve the fluorescence of CPDs [49], [81], [82].

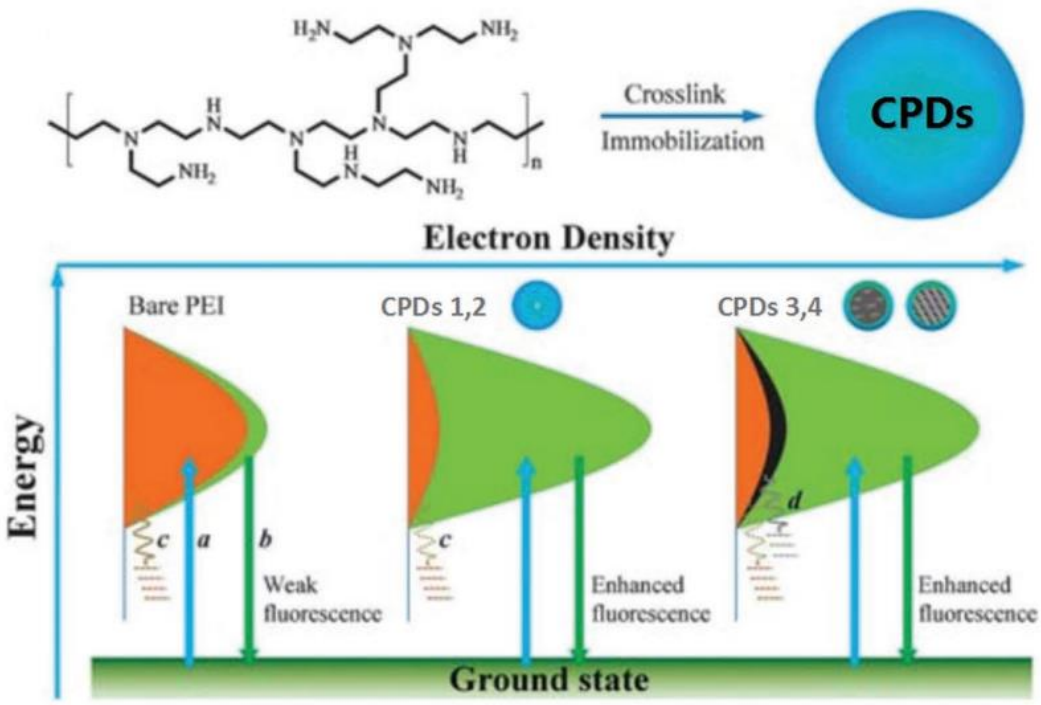

Figure 13. Schematic representation for CEE effect of bare Polyethyleneimine and CPDs. (Reproduced with permission, source [49]).

Regarding the fifth point of the list, CPDs may have some specific molecular structures incorporated in the polymer/carbon hybrid skeleton, which serve as fluorescence centres to enhance PL just as the organic fluorescent molecules [49]. This PL mechanism is related to what is called '*molecule state' (V)* [53]. Ehrat et al. have identified derivatives of citrazinic acid, blue-emitting fluorophores, as responsible for the enhancement of the PL [83]. These fluorophores can be incorporated to structure of CDs or bound to surface [36]. In fact, especially with regard to CDs produced mainly through bottom-up routes where nucleation

and growth mechanisms take place, it is possible that molecular intermediates (often pyrydone-like structures) are formed during reactions, leading to emission spectra expansion, which may generate confusion as to the real properties of this type of CDs [62].

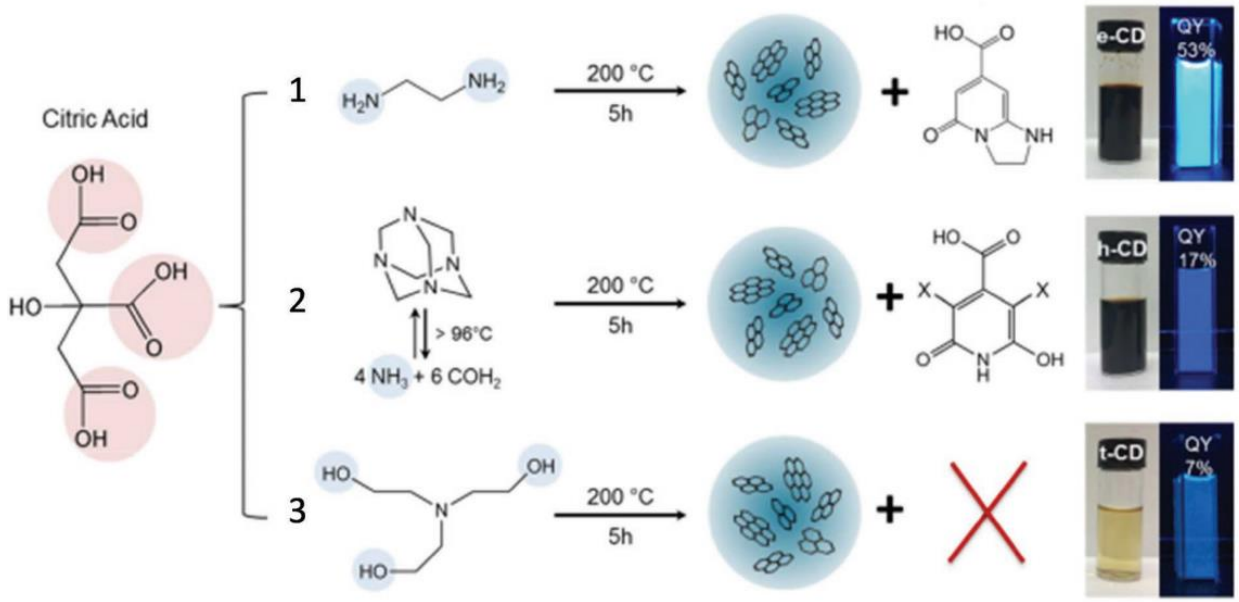

Figure 14. Schematic diagram of synthesis process of citric acid–based CPDs using three different nitrogen-containing precursors. The molecular state produced in reaction 1 (IPCA reported in previous work) and reaction 2 (citrazinic acid and/or 3,5 derivatives (marked by −X)) contribute to the bright luminescence. In reaction 3, there isn't molecular state produced resulting in low PLQY. (Reproduced with permission, source [49]).

Lastly, there are some *parameters (VI)* influencing the PL of CDs, like pH and temperature. The pH-dependent fluorescence of PDs further confirms that an acidic environment results in a much more rigid and compact conformation and enhance fluorescence. Lu et Al. demonstrate that their CDs polymer-based were influenced in morphology and optical properties by the decrease of pH. In fact, according to them, H^+ ions could serve as a catalysis to promote dehydration reaction and increase carbonization degree [84]. Additionally, higher temperature and longer reaction time also contributes to a higher carbonization degree and more effective graphitization, resulting in larger conjugation structure, which leads the bandgap to become narrower with possible red-shift emission [49],[61].

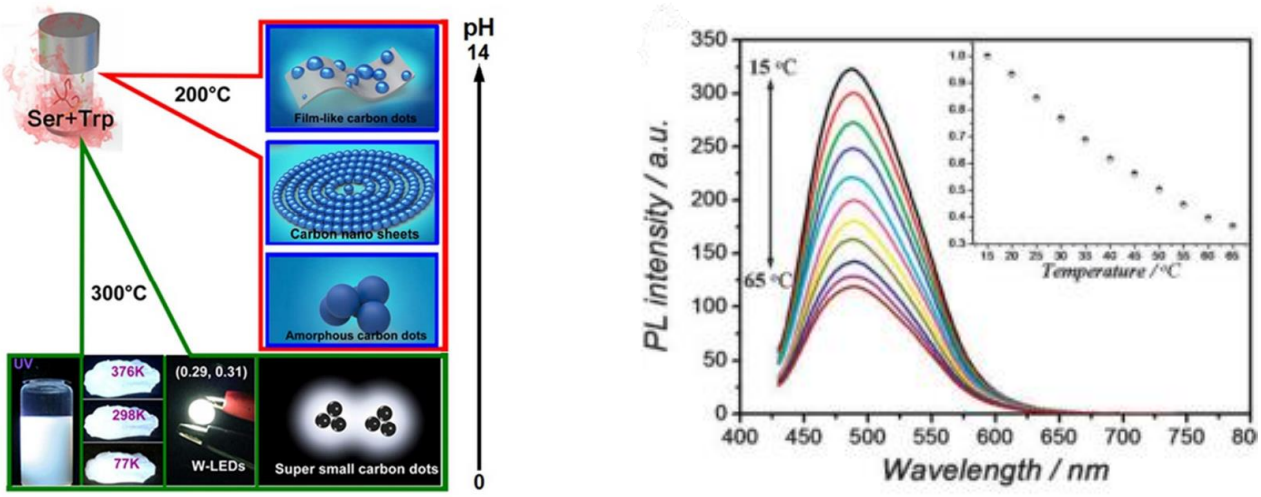

Figure 15. On the left, the pH-dependent structures of CPDs. (Reproduced with permission, source [84]). On the right, the temperature-dependent photoluminescence of CPDs. (Reproduced with permission, source [61]).

1.2.4 Radical scavenging activity of CDs

Among other applications, as mentioned in **section 1.2.1,** CDs are employed as antioxidants since they have been shown to possess ROS scavenging activity. Many studies have been done to explain the mechanism by which CDs achieve this purpose. The answer can be found considering their structure. Having a fairly extensive sp^2 carbon network in the core, CDs can act as electron storage and transfer electrons to ROS, transforming them into a less reactive and dangerous chemical entity [6],[85]–[87].

Another way to deactivate ROS is 'adduct formation', also due to sp2 domains, and which consist in an addition reaction which involves ROS and sp^2 network of CDs, followed by a delocalization of spin across the conjugated graphene-like core [6],[86]–[88]

The third mechanism which explain how CDs can deactivate ROS is the 'hydrogen donation' from functional groups situated on the edge sites of CDs, like OH, COOH, SH and NH_2, which dramatically increase with heteroatoms doping [87], [6], [88], [89].

Ultimately, mechanisms through which CDs interact with radicals inhibiting their dangerous reactivity are similar to those viewed in both **sections 1.1.1 and 1.1.2** for natural and synthetic antioxidants. Below, there are two illustrations of these three aforementioned mechanisms.

a) b)

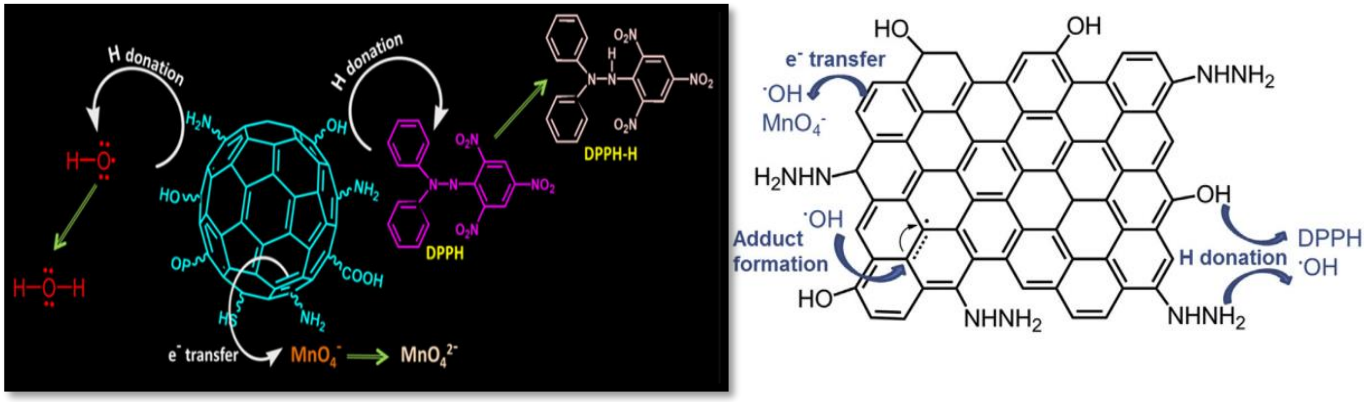

Figure 16. a) Mechanism of the antioxidant activity of nitrogen, phosphorous and sulfur codoped CDs (NPSC-dots). (Reproduced with permission, source [88]). b) Mechanism for antioxidant activity of GQD. (Reproduced with permission, source [86]**)**.

Wanting to go deeper into the matter, Getachew et al. [28] investigated the influence of doping with heteroatoms on CDs scavenging ability using two other atoms-based dopants: Cu and Cl. They demonstrated that scavenging capability of CDs dramatically decreased, since they could disrupt the intrinsic sp^2 hybridized structure and substantially reduce the interaction between free radicals and C=C bonds of CDs core. Another motivation they gave was the decline in functional groups with strong hydrogen donors in the CuCl-CDs caused by coordination interactions between Cu^{2+} ions and carboxylate (or hydroxyl) groups at the edge sites of the CDs. Instead, they noted that doping with these 2 heteroatoms led to an increase in ROS generation, making them potential candidates in photodynamic therapy to treat cancers (e.g., esophageal and lung cancers), skin diseases (e.g., hypertrophic scars, age-related macular degeneration and actinic keratoses), and diseases induced by pathogenic bacteria or biofilm (e.g., periodontitis and dental cavities) [28].

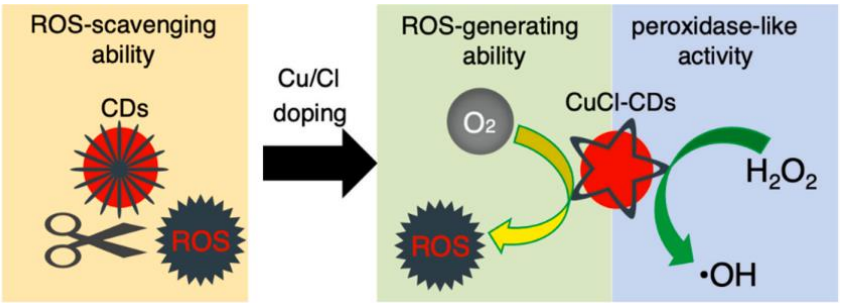

Figure 17. Schematic illustration of CDs with ROS scavenging ability and CuCl-CDs with ROS generation capability and peroxidase-mimic activity. (Reproduced with permission, source [28]).

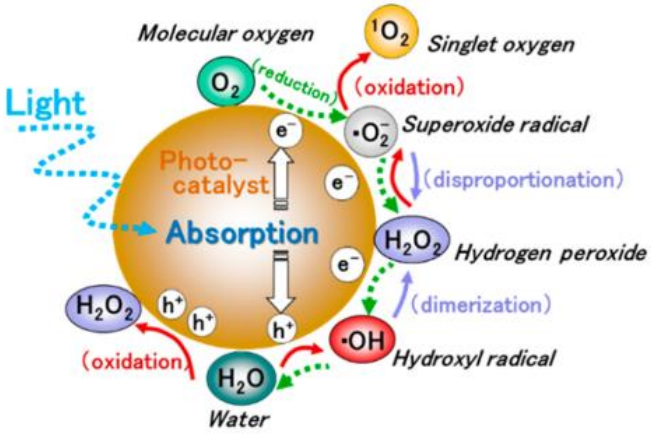

Figure 18. Reactive oxygen species generated in the photocataytic reduction and oxidation steps of oxygen and water. (Reproduced with permission, source [90]).

CHAPTER 2 MATERIALS AND METHODS

2.1 Materials: reagents and instrumentation

The reagents used for the synthesis were Citric Acid (CA), p-Phenylenediamine (DPA), Methylene Blue (MB), Cochineal Red (CR), deionized water. Curcumin was used for the evaluation of radical scavenging activity.

The instruments used for the synthesis, weighing and grinding were respectively: a Vibra Cell sonicator purchased from Sonics, an analytical balance of Radwag and a mortar.

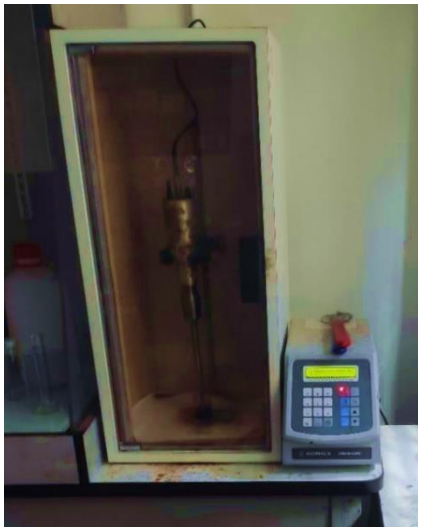

Figure 19. Vibra Cell sonicator purchased from Sonics.

An oven was employed for drying step, while for what concern the purification one the instruments used were: a VELP Scientifica magnetic plate and a dialysis membrane with cut-off value of 3.5 kDa.

CDs were then analysed through Nicolet 5700 Fourier-transform infrared spectrometer from Thermo Fisher Scientific as regards FT-IR spectroscopy. Photoluminescence spectra were instead obtained through PerkinElmer LS-55 fluorescence spectrometer.

Figure 20. Nicolet 5700 Fourier-transform infrared spectrometer (on the left) and PerkinElmer LS-55 fluorescence spectrometer (on the right).

UV/VIS absorbance spectra were acquired through the PerkinElmer Lambda 35 UV/VIS spectrometer. For UV/VIS analysis and fluorescence ones, Hellma quartz cuvettes were utilised. Regarding X-ray photoelectron spectroscopy analysis, PHI 5000 Versa Probe instrument (Physical Electronics) equipped with an Al Kα radiation (1486.6 eV) X-ray was employed.

Figure 21. PerkinElmer Lambda 35 UV/VIS spectrometer

Lastly, a UV lamp (VIQUA S463RL) and a rudimentary chamber consisting of a cardboard box (41 cm x 25.5 cm, L x W) and tin foil were employed in order to irradiate samples and evaluate radical scavenging activity. The irradiation condition applied was 0.037 W/cm^2.

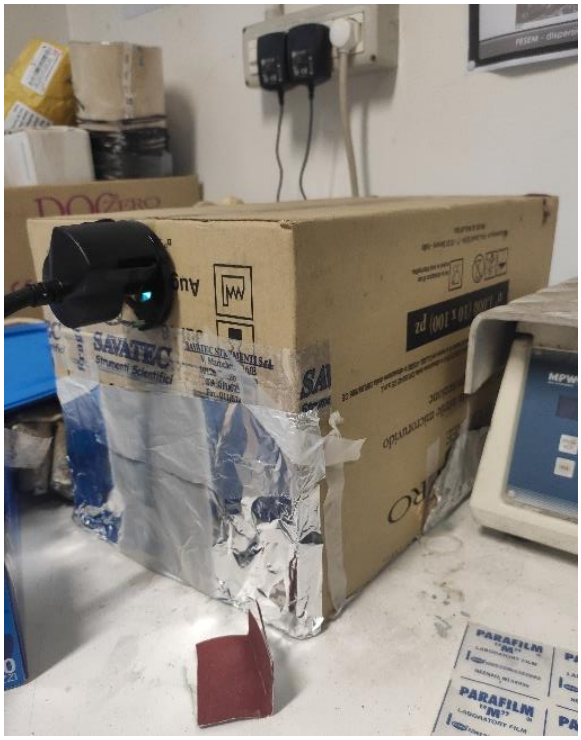

Figure 22. A picture of the rudimentary chamber for radical scavenging test.

2.2 Methods

2.2.1 Synthesis and purification of pristine CDs

For the synthesis of CDs, reference was made to the article of Mintz et al. [91], trying as best as possible to respect the indicated proportions between the quantities of reagents.

Therefore, for sample 1, 760 mg of p-DPA were taken and mixed with 54 mg of CA with the aid of a mortar. Then, 14 mL of deionised water were added to the preparation. The solution was subsequently sonicated for 1 hour at 42 kHz (subsequence of 30s and 10 on and off). Afterwards, the solution of CDs was purified through dialysis with the use of a membrane with cut-off of 3.5 kDa so that molecules smaller than 3.5 kDa could permeate. To better succeed in purification, dialysis was performed on a magnetic stirrer for 48 h, changing water after 24 h.

Lastly, membrane was open, and solution was poured into a beaker and dried in an oven at 60 °C for 72 hours.

Figure 23. Pristine CD preparation after drying.

For both samples 2 and 5, quantities of reagents were altered, while keeping the proportions between them unchanged. In fact, 660 mg of p-DPA were added to 47 mg of CA and mixed as before, keeping the proportion between them equal to 1:14. The same was made for deionised water, keeping the proportion between it and p-DPA equal to 1:56. Following process steps remained the same too.

Regarding sample 3 and sample 5, quantities of reagents were changed again: 560 mg of p-DPA, 40 mg of CA and 10 mL of deionised water were chosen slavishly following Mintz et al. work. The only difference concerned the dialysis time to which sample 3 was subjected

(24 h and not 48 h). Even for them, the other process steps remained the same. In table 1, there is a schematic illustration summarising synthesis process together with characterization ones which will discussed later.

Table 1. An illustration of main synthesis and characterization steps of pristine CDs.

CD_1	CD_2	CD_3	CD_4	CD_5
760 mg p-DPA	660 mg p-DPA	560 mg DPA	560 mg DPA	660 mg DPA
54 mg CA	47 mg CA	40 mg CA	40 mg CA	47 mg CA
14 mL H20	12 mL H20	10 mL H20	10 mL H20	12 mL H20
48h dialysis	48h dialysis	24h dialysis	48h dialysis	48h dialysis
Oven 60° C 72h	Oven 60° C 72h	Oven 60° C 72h	Oven 60° C 72h	Oven 60° C 72h

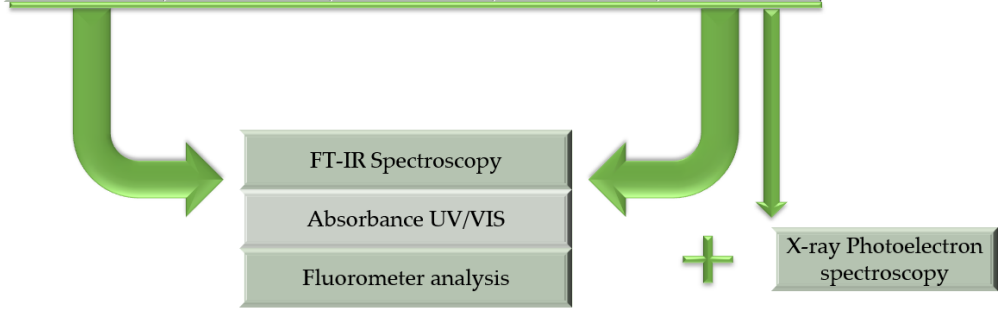

2.2.2 Synthesis and purification of CDs conjugated with Methylene Blue and Cochineal Red

As to conjugated CDs with the two dyes (Methylene Blue and Cochineal Red), synthesis steps remained almost the same, the only difference being that the two powder dyes were added in an amount equal to 5 % by weight of p-DPA. In this case, for both types of conjugated CDs, the quantities of reagents chosen were: 660 mg of p-DPA, 47 mg of CA, 33 mg of dye powders (Methylene Blue for the first ones and Cochineal Red for the second ones).

Figure 24. A detail of Methylene Blue added to CA and p-DPA and mixed with a mortar.

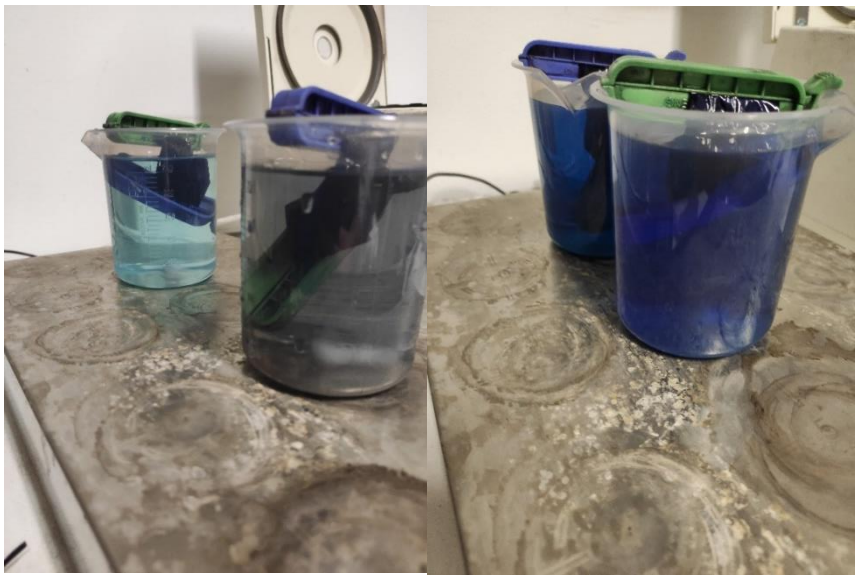

Figure 25. Dialysis of two CDs preparations with Methylene Blue hours away.

Below it's possible to see two schemes summarising synthesis process and characterizations processes to which the samples were subjected and that will be discussed later.

Table 2. An illustration of main synthesis and characterization steps of CDs conjugated with Methylene Blue.

CD + Meth Blue_1	CD + Meth Blue_2	CD + Meth Blue_3
660 mg DPA	660 mg DPA	660 mg DPA
47 mg CA	47 mg CA	47 mg CA
33 mg Methylene Blue	33 mg Methylene Blue	33 mg Methylene Blue
12 mL H20	12 mL H20	12 mL H20
48h dialysis	48h dialysis	48h dialysis
Oven 60° C 72h	Oven 60° C 72h	Oven 60° C 72h

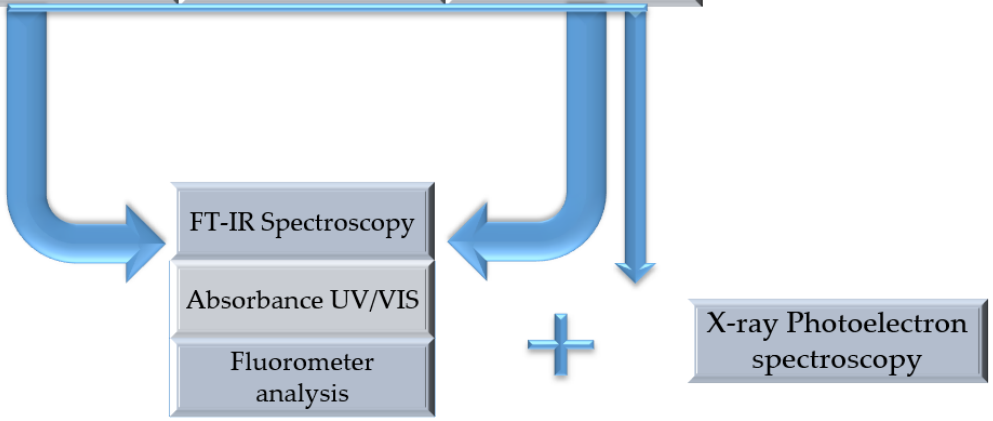

Table 3. An illustration of main synthesis and characterization steps of CDs conjugated with Cochineal Red.

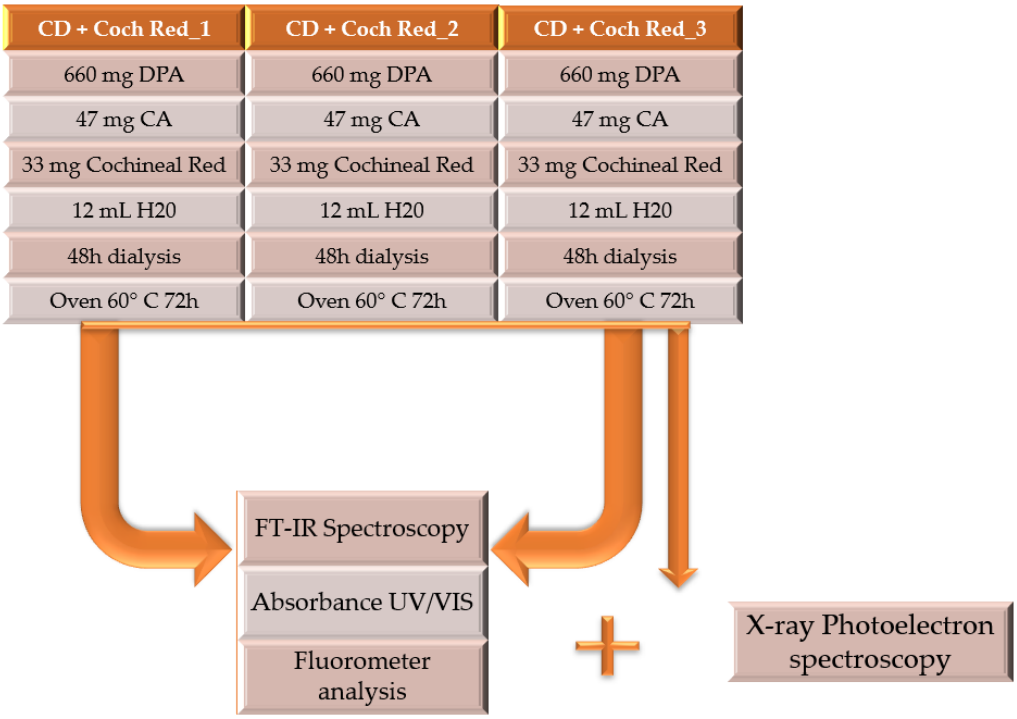

2.2.3 FT-IR spectroscopy

For what concern CDs characterization, first analysis performed was FT-IR spectroscopy in order to investigate surface of the samples and to understand what kind of reactions occurred between the precursors during the formation of compounds. The acquisition number chosen for spectrum sampling was 64 and range selected was 500 cm^{-1} – 4000 cm^{-1}. Before obtaining CDs spectra, a background sampling of the air present in the laboratory was first performed, in order to subtract the related contributions from the spectrum of the CDs. Lastly, baseline correction and normalization were carried out. The spectra were then elaborated with Origin 2023.

2.2.4 UV/VIS analysis

UV/VIS analysis were performed using 380 nm-800 nm as wavelength range, meaning from visible light to near-IR. UV/VIS spectra were collected for 3 different reasons:

I. To assess if the dyes reacted well and if they bonded with the other two precursors;
II. To obtain information about the delocalization of π-system and its diffusion through the structure of CD;
III. To perform Curcumin degradation/prevention test.

First aim (I) was achieved evaluating and comparing the specific peaks of each species.

Second one (II) has been achieved by correlating the values of absorbance obtainable from the spectra and a gaussian parameter, σ, which expresses in eV the width of the conduction and valence bands, related to the extension/diffusion of the π cloud in the structure, which can be influenced and modified by the various solutions proposed in **section 1.2.4.**

Figure 26. Blanks of Cochineal Red (on the left) and of Methylene Blue (on the right) before UV/VIS analysis.

In particular, considering Lambert-Beer law,

$$A = \rho\, \varepsilon_\lambda\, l \qquad [1]$$

(where A is the absorbance, ρ is the mass concentration and l is the optical path)

it is possible to obtain mass extinction coefficient ε_λ by plotting absorbance against solution concentration (three solutions at different concentrations were prepared with as many relative absorbance peaks) and then imposing an interpolating line forced at the axis origin, whose slope corresponds to mass extinction coefficient times the optical path length, $\varepsilon_\lambda l$.

Dividing this value for l (1 cm in our case), ε_λ is found.

After this, the absorption coefficient α was obtained through the following formula:

$$\alpha = \frac{4\pi\varepsilon_\lambda}{\lambda} \quad [2]$$

(where λ are the wavelengths (in nm) corresponding to maximum peak intensity for each emission curve obtained from fluorescence analysis as will be seen later in **section 2.2.5.)**

Then, natural logarithm of α was calculated and plotted against the energies (in eV) of emission curve. A fitting with a parabolic interpolation was performed and the second order coefficient of the interpolated curve was taken as "a" coefficient. Lastly, according to the following equations, σ was found:

$$a = \frac{1}{4\sigma^2} \quad [3]$$

And, consequently:

$$\sigma = \frac{1}{\sqrt{4a}} \quad [4]$$

Results of σ will be shown in chapter 3.4, after fluorescence analysis will be completed and discussed.

Concerning third aim (III), this test was performed in order to evaluate CDs antioxidant properties / radical scavenging capability.

To this end, firstly, three solutions of Curcumin with deionised water at different concentrations were prepared (0.0333 mg/mL, 0.02 mg/mL and 0.01 mg/mL) and analysed through UV/VIS spectrometer before and after 30 minutes UV light irradiation. In this way, a calibration line was obtained plotting absorbance against concentrations as seen before, taking the slope of the curve as $m=\varepsilon_\lambda l$.

Subsequently, the concentration of Curcumin degraded by irradiation was calculated as follows:

$$C'' = \frac{A''}{m} \quad [5]$$

(where C'' represents the concentration of degraded Curcumin after irradiation and A'' the absorbance peak of Curcumin after irradiation).

Then, degradation of Curcumin alone (D_{alone}) was estimated using the following equation:

$$D_{alone} = \frac{C''-C\prime}{C\prime} \quad [6]$$

(where C'' represents the concentration of degraded Curcumin after irradiation and C' the concentration of Curcumin before irradiation).

After that, solutions with CDs (both pristine and conjugated with MB and CR), curcumin and deionised water were prepared (concentrations will be revealed in **chapter 3**) and analysed pre and post UV light irradiation as was done for Curcumin alone. Thus, through absorbance peaks obtained from the spectra before and after irradiation and using the same m coefficient, the concentration of Curcumin degraded by irradiation was estimated according to the following equations:

$$C_2 = \frac{A_2}{m} \quad [7]$$

(with C_2 representing the concentration of degraded curcumin in solution with CDs after irradiation and A_2 the absorbance peak of Curcumin in solution with CDs after irradiation).

At this point, degradation of Curcumin with CDs (D_{CC}) was estimated using the following equation:

$$D_{CC} = \frac{C_2 - C_1}{C_1} \quad [8]$$

(where C_2 and C_1 represent the concentration of curcumin before and after irradiation respectively)

In this way, the preservative action of carbon dots, expressed in %, could be assessed, and, to this end, the following equations were employed:

$$Prevention\ (\%) = 100 - \left(\frac{D_{CC}}{D_{alone}}\right) \times 100 \quad [9]$$

Where the second term of the equation after the minus sign represents the degradation that Curcumin undergoes when protected by the antioxidant action of carbon dots compared to when it is alone and unprotected.

Also in this case, the spectra were then elaborated with Origin 2023.

Figure 27. Three solutions of Curcumin alone at different concentrations are shown during the irradiation.

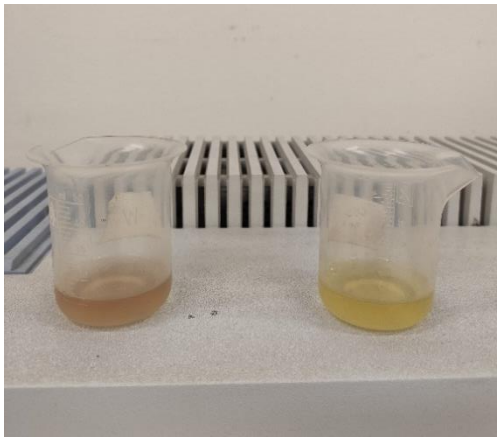

Figure 28. On the left, a solution of CD and Curcumin irradiated is shown. On the right, a solution of CD and curcumin before irradiation.

2.2.5 Fluorometer analysis

In order to evaluate the fluorescence emission response of CDs, which among other things is important for assessing a possible biomedical application in photothermal therapy or in-vivo imaging, it was decided to excite with 9 wavelengths from 240 nm (5.167 eV) to 300 nm (4.133 eV), in steps of 10 nm. The entrance and exit slits were imposed to be 5 nm, while scan speed 50 nm/s, with the intent to obtain more accurate measurements.

First of all, blanks spectra of the two dyes were obtained. For what concern Methylene Blue, spectrum was obtained from OMLC database. Then, solutions of CDs (pristine ones and conjugated ones) were prepared at different concentrations (ranging from 0.01 to 0.1

mg/mL) trying to reach a good compromise between a too concentrated solution which would then obstruct the light beam, and a too diluted solution, which would have produced a fluorescence response too similar to that of plain deionised water and therefore too noisy. Again, the spectra were elaborated with Origin 2023, thanks to which graphs were also obtained plotting the position of the emission peaks expressed in eV against the laser excitation energy of the instrument also expressed in eV, allowing the σ evaluations expressed in section 2.2.4 *(aim II)* to be performed.

2.2.6 X-ray Photoelectron Spectroscopy

With regard to X-ray Photoelectron Spectroscopy (XPS), the instrument used was a PHI 5000 Versa Probe instrument (Physical Electronics) equipped with an Al Kα radiation (1486.6 eV) X-ray.

In order to obtain the spectra, first of all, a baseline was subtracted selecting 'XPS' as 'baseline mode' and then 'Shirley' or 'Tougaard' as method, depending on the quality of the result obtained with either method. Then, the obtained y-axis was normalised and, using 'Gaussian' as 'peak function', fitting was performed and then manually adjusted.

CHAPTER 3 RESULTS

3.1 Synthesis process

As regards pristine CDs, they were obtained using CA and p-DPA as precursors, following the procedure described in the work of Mintz et al.[91], through which it is possible to speculate on the growth mechanism concerning the reactions between precursors. Here there is a schematic representation of the supposed growth mechanism, taken from the work of Pidkova Solomiya [92]:

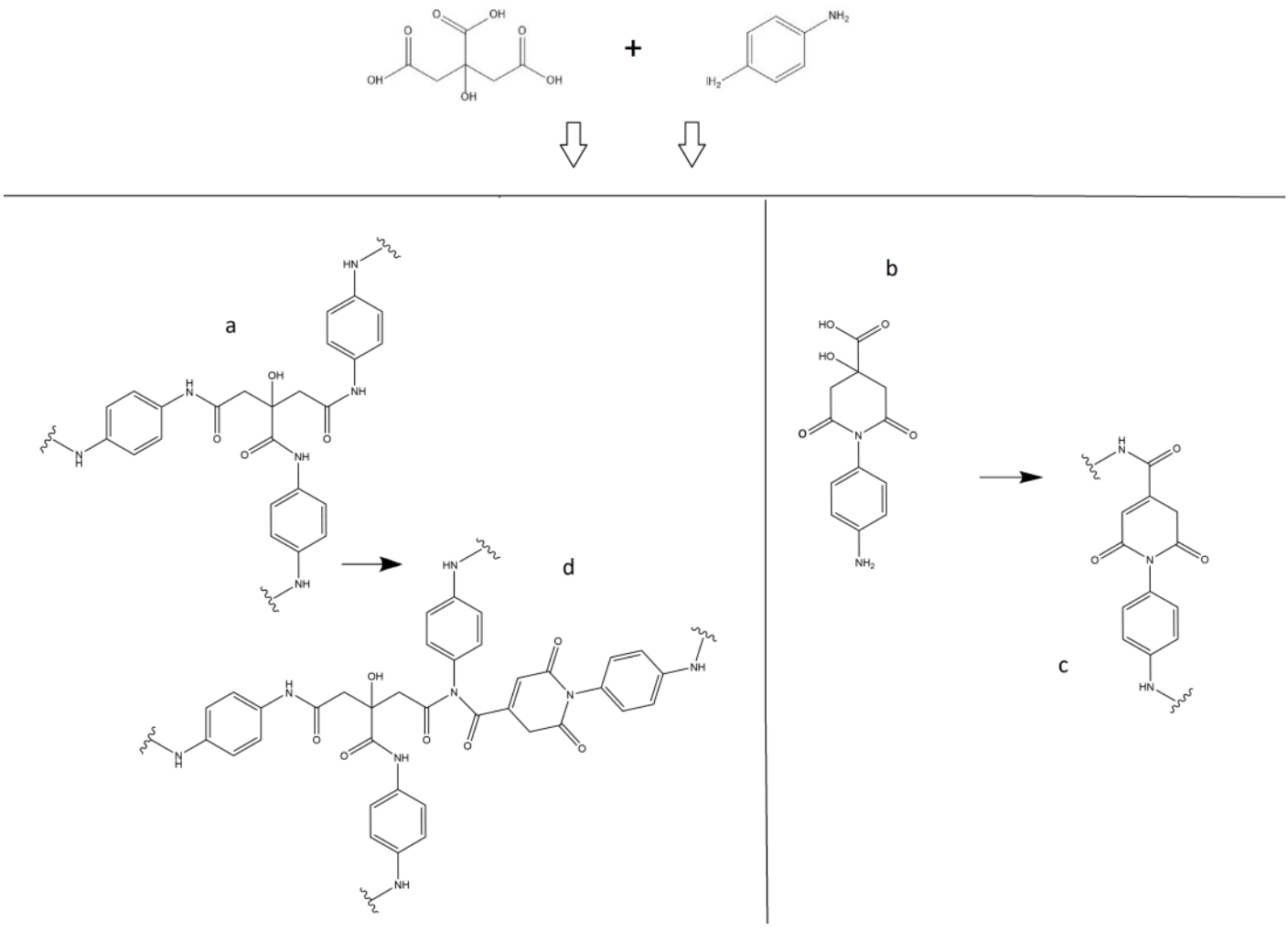

Figure 29. Supposed growth mechanism of the synthetized CDs, with citric acid and p-DPA as precursors (on the top). (Source: [92]).

On top it is possible to see the structures of the two precursors (CA and p-DPA). In *Figure 29* it's possible to see how CA can react with p-DPA to initially form amide derivates followed by the formation of polymeric structures, which leads us to classify our carbon dots as CPDs (see **section 1.2.3**, IV). In addition, it is possible to assume that CA is induced to condense and form a heterocyclic structure favoured by water elimination reactions and that amine groups of p-DPA can react with two CA carboxylic functionalities leading to the formation of cyclic unsaturated amine functionalized on nitrogen atom with p-DPA residue and a carboxylic functionality (*Figure 29*, *b-c*). This can react again with CA and leading to the formation of more complex structure and so on.

Below there is a schematic illustration of a hypothesized structural model of a CPD given by Mintz et al. [91], with the only difference that o-DPA instead of p-DPA was used in these considerations:

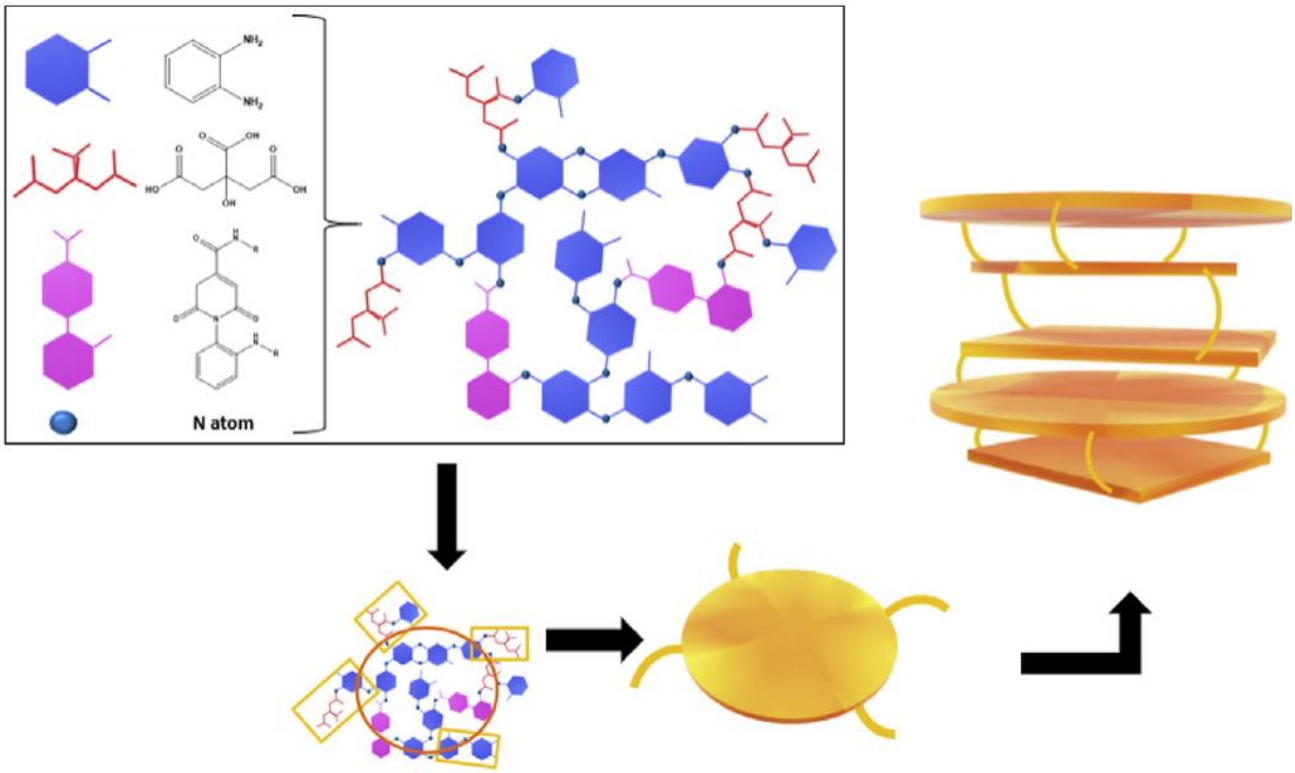

Figure 30. Supposed structural model of CPDs. (Reproduced with permission, source [91]).

3.2 FT-IR Spectroscopy

Regarding FT-IR analysis, building on the above considerations on growth mechanisms, it is possible to see if and how these have been completed, thanks to the study of the position of the characteristic stretching and bending peaks of the most important functional groups. We will start from discussing the precursors spectra.

Considering CA, starting from the lower energies, it's possible to see the most important functionalities of this carboxylic acid. At 3200-3500 cm^{-1} there are two peaks corresponding to the stretching of OH, in particular, the first is related to hydroxyl ν_{OH} and the second to carboxylic ν_{OH}. The peak at 2900-3000 cm^{-1} refers to the saturated ν_{C-H}. In the region of 1660-1800 cm^{-1} it is possible to see the characteristic peak of the carbonyl group stretching $\nu_{C=O}$.

As for p-DPA IR spectrum, peaks related to stretching of NH can be observed at 3200-3400 cm^{-1}, with the first ones likely to be attributable to a primary amine, and the second one to a secondary/tertiary amine. At 2900-2950 it is possible to see a peak typical of the aromatic compounds, corresponding to the unsaturated ν_{C-H}. In the region of 1600-1700 cm^{-1} there is a peak referring to the bending δ_{C-N}. At 1550 cm^{-1} there is a peak attributable to $\nu_{C=C}$, while in the region 1250-1350 there is a peak representing ν_{C-N}.

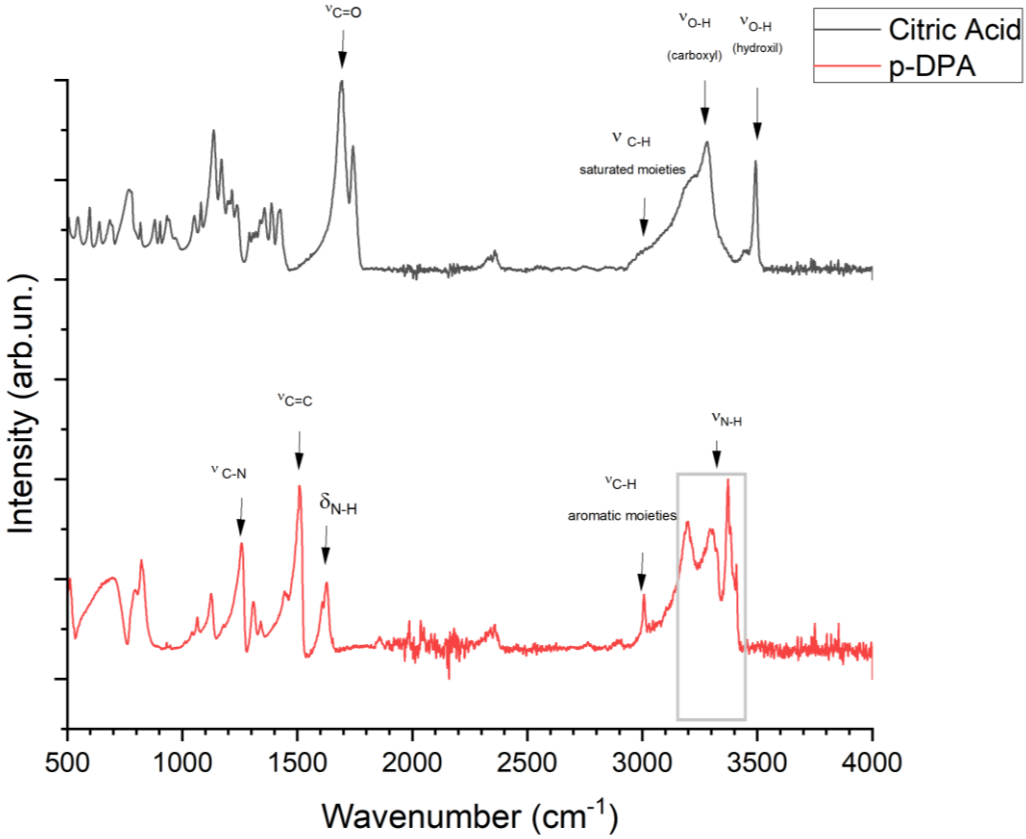

Figure 31. FT-IR spectra of CA and p-DPA.

Now, let's start focusing of pristine CDs spectra. Comparing these with the spectrum of CA, it can be notice that, in each sample, the peak related to the hydroxyl OH disappears, indicating that CA reacted. Additionally, the peak related to the saturated ν_{C-H} decreases in intensity (less in sample 3 and 4), indicating the formation of aromatic structures. Lastly the peak characteristic of carbonyl group $\nu_{C=O}$ decrease in intensity too, suggesting that they reacted with the amine groups of p-DPA.

Comparing them instead with p-DPA spectrum, it's possible to see that peaks of NH stretching remain (particularly visible in sample 1 and sample 5), changing a bit their proportions and intensity, probably indicating that reactions between amino groups of p-DPA and carboxyl groups of CA occurred, transforming them into amides. It is still possible to see peaks related to the unsaturated ν_{C-H} (highly visible in sample 3 and 4), because they are still present in amides, as those referring to ν_{C-N}, to which are added the peaks referring to $\nu_{C=N}$ at approx. 1500 cm^{-1}, and indicating another possible mode of bonding between C and N.

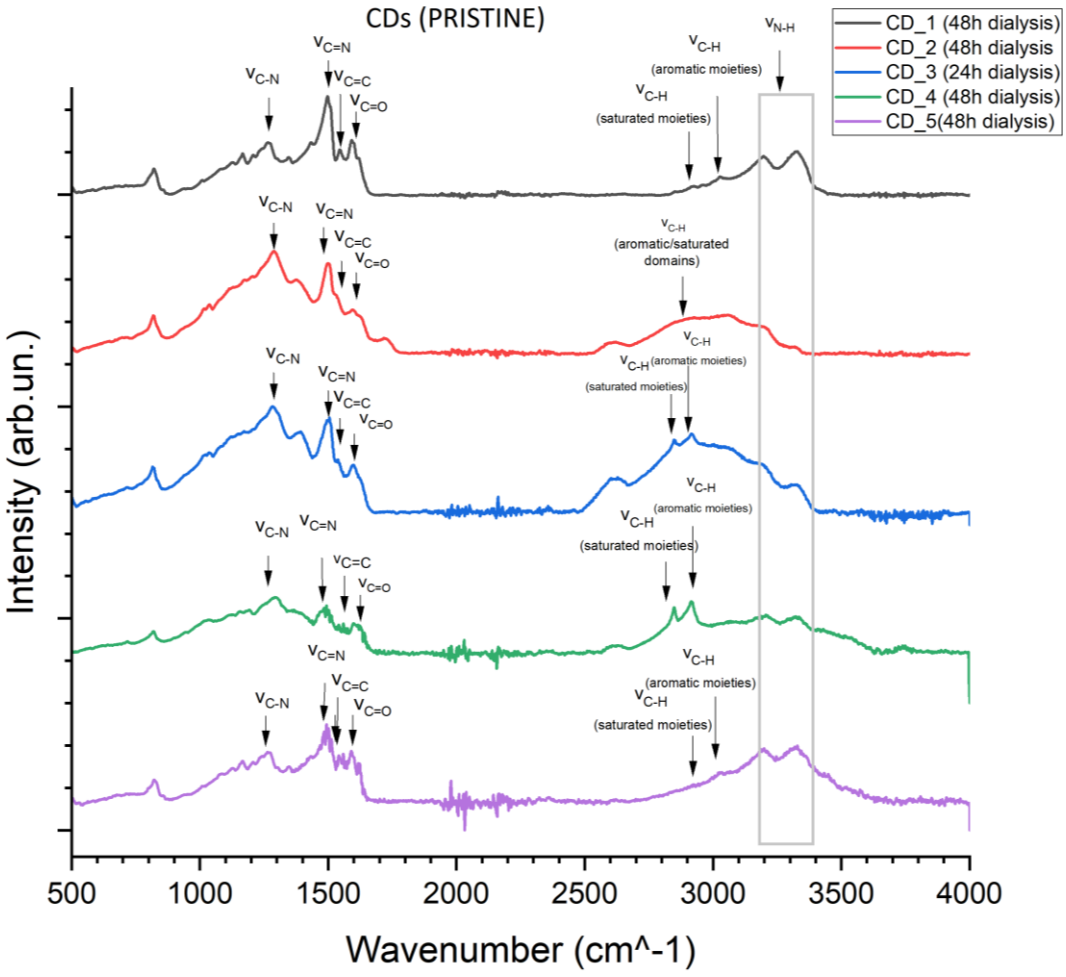

Figure 32. FT-IR spectra of pristine CDs.

Moving on the dye-conjugate samples, let's shift the focus on the influence of Methylene Blue and Cochineal Red on sample spectra and it will be speculated how it might influence the reaction mechanism. Below, structures of Methylene Blue and Cochineal Red are reported.

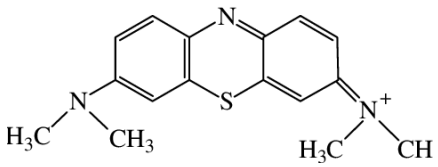

Figure 33. Structure of Methylene Blue.

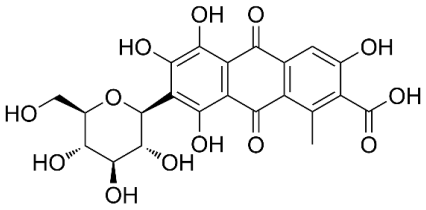

Figure 34. Structure of Cochineal Red.

In *Figure 35* blanks spectra of the two dyes are reported with their relative molecular vibrations of the various chemical bonds.

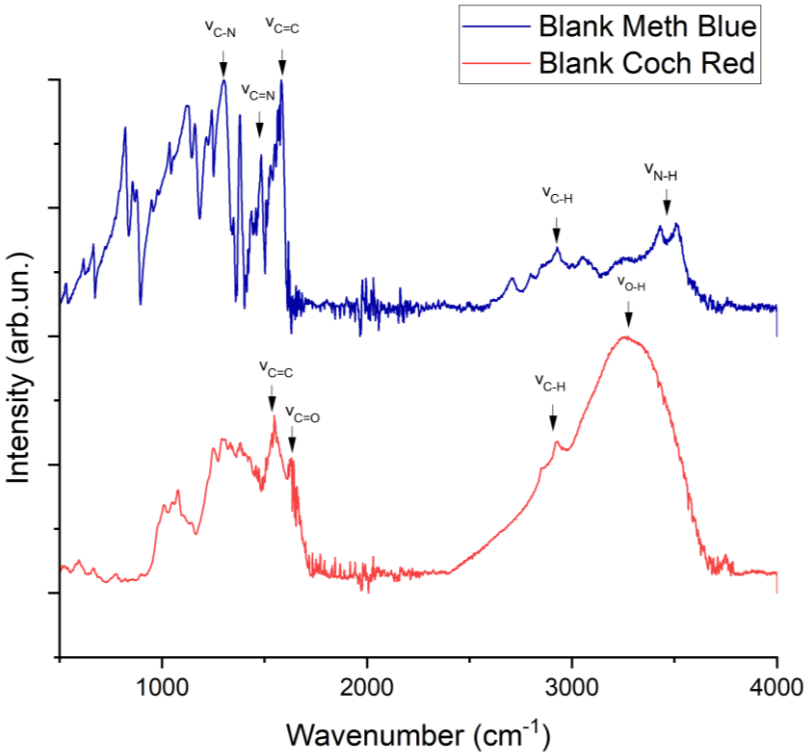

Figure 35. FT-IR spectra of Methylene Blue and Cochineal Red

In the following, graph with all MB-conjugated samples is shown. As only 5% by weight of dye was added to the preparation, the peaks remained virtually unchanged, although more pronounced C=N and C-N stretching peaks were noted, probably due to the aromatic ring typical of methylene blue, which exhibits these bonds. As it possible to see in *Figure 33*, Methylene Blue presents a Nitrogen atom positively charged and may lead to nucleophilic addition reactions with carboxyl group of CA.

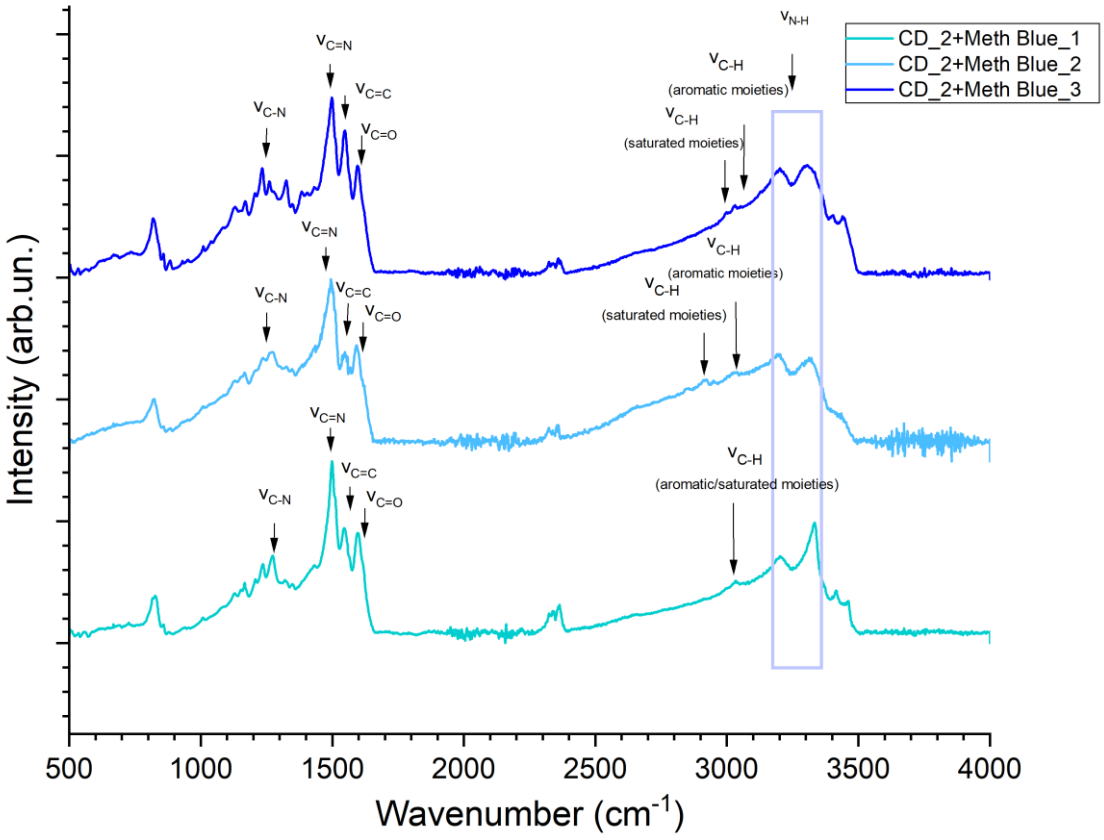

Figure 36. FT-IR spectra of MB-conjugated samples.

Below, FT-IR spectra of CR-conjugated ones are displayed.

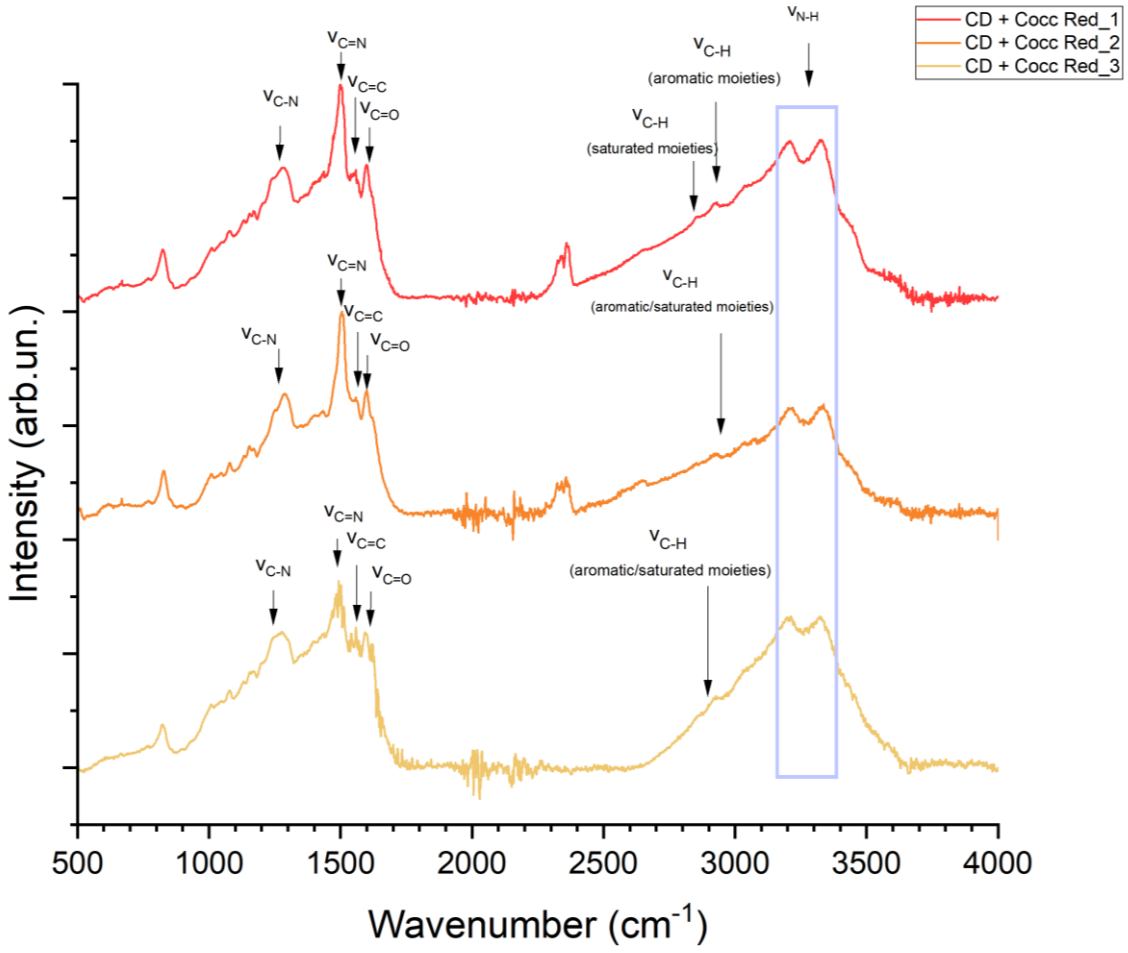

Figure 37. FT-IR spectra of CR-conjugated samples.

Even in these spectra there are not so many differences regarding positions and intensities of the peaks, but, taking into account structure of Cochineal Red, esterification reactions between the COOH of the Cochineal Red and OH of CA, or between two COOH (one from the CR and the other one from the CA) can be assumed to occur, resulting in esters or anhydrides.

3.3 UV/VIS analysis

Firstly, the UV/VIS spectrometer was employed in order to obtain information about the attachment or non-attachment of the two dyes (MB and CR) to CDs. For this purpose, all CDs (pristine and dye-conjugated ones) were analysed in solution with water at different concentrations. Pristine ones showed maximum peaks at 514 (sample 4) - 550 nm (sample 3). From now on, only the spectra of one sample per type will be reported in order to save space and facilitate reading. In this case, only spectrum of pristine sample 3 is reported.

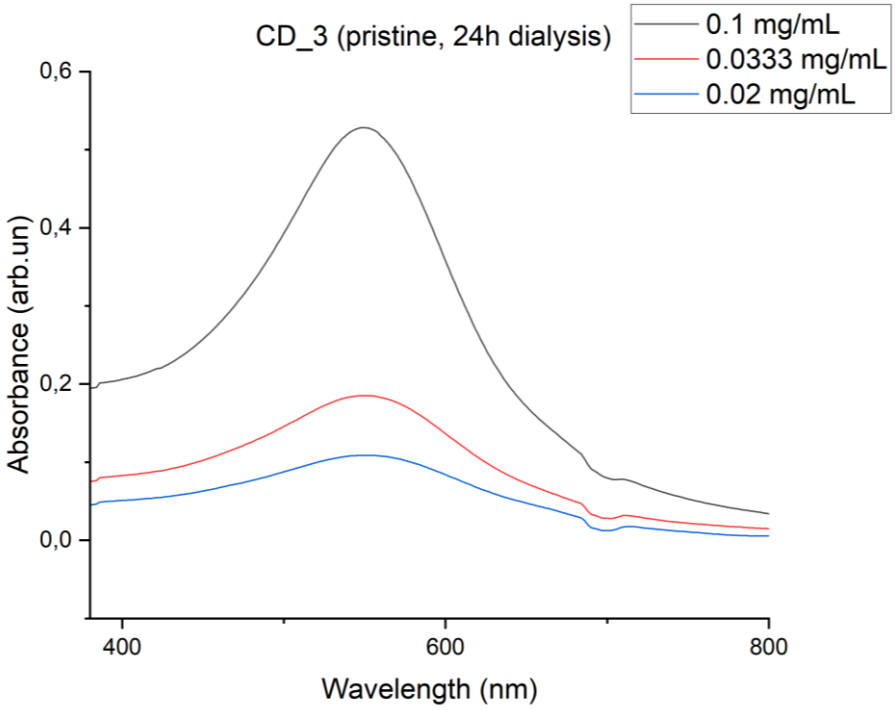

Figure 38. Pristine sample 3 UV/VIS spectrum at different concentrations.

After that, measurements of dye-conjugated samples were collected, and spectra interpreted. For this purpose, blanks measurements of the two dyes were first made as illustrated below in the following graphs, in which, regarding Methylene Blue, a shoulder at 614 nm and a maximum peak at 664 nm can be observed. For what concern Cochineal Red blank, two peaks respectively at 516 and 554 nm can be noticed.

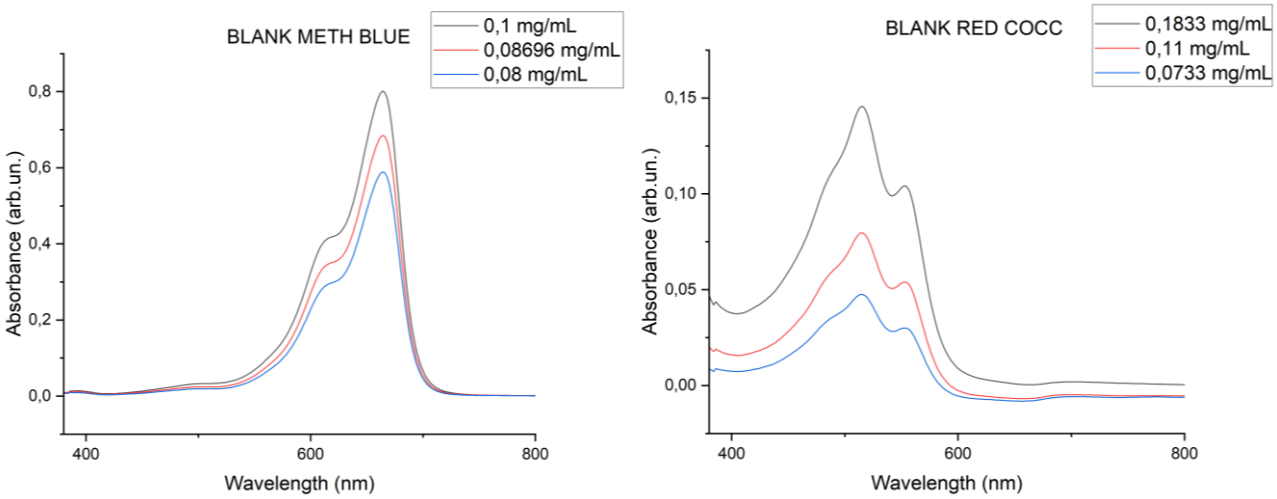

Figure 39. Blanks UV/VIS absorbance spectra (methylene blue on the left and Cochineal Red on the right).

Analysing MB-conjugated samples, and, in particular, that of MB-conjugated sample 2 reported below, it's possible to notice a clear peak related to the dye, which can be spotted at approx. 660 nm.

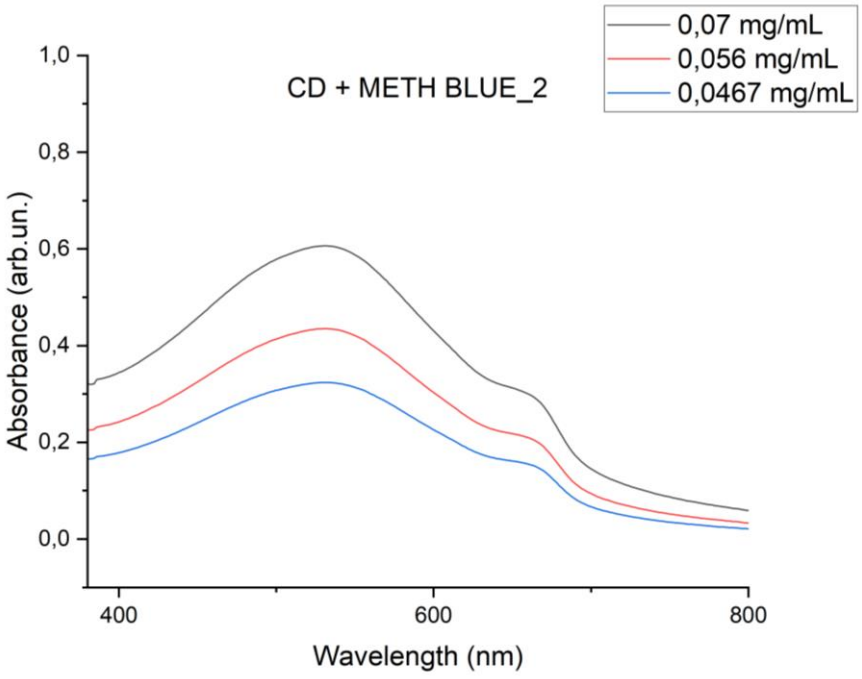

Figure 40. UV/VIS absorbance spectra of Methylene Blue-conjugated sample 2.

Concerning Cochineal Red-conjugated ones, UV/VIS absorbance measurements were not very helpful because Cochineal Red has a characteristic peak superimposed on that of pristine CDs, even if (especially in sample 2 which is the only one reported below) there is a change in the shape and appearance of the peak at around 550 nm, which appears more spangled and asymmetrical than before, probably affected by the presence of the higher of the two peaks characteristic of Cochineal Red.

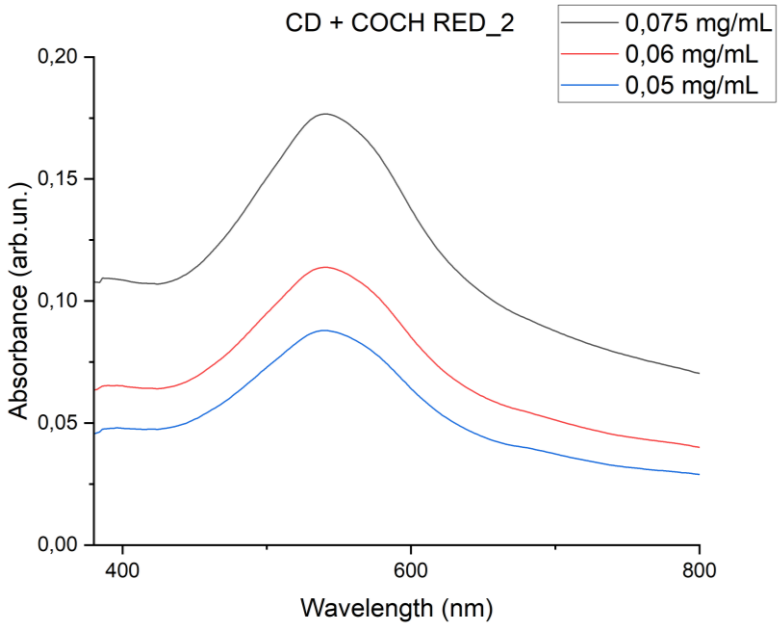

Figure 41. UV/VIS absorbance spectra of Cochineal Red-conjugated sample 2.

Results regarding the other two aims discussed in **section 2.2.4** will be discussed later in **section 3.4** and **section 3.5** respectively.

3.4 Fluorometer analysis

Results from fluorescence analysis are reported below. First of all, blanks spectra of Methylene Blue and Cochineal Red (for the latter, excitation wavelengths: 240– 320 nm) are reported in order to identify characteristic emission peaks. It's possible to see that there are three peaks for Methylene Blue, whose highest is situated at 1.87 eV (664 nm), while second one at 4.25 eV (292 nm) and third one at 5.04 eV (246 nm). In particular, first one will be really visible in MB-conjugated CDs spectra and will be the one on which we will focus our attention.

Instead, regarding Cochineal Red, an unique peak placed at 2.79 eV (444 nm) is present in the range of our interest.

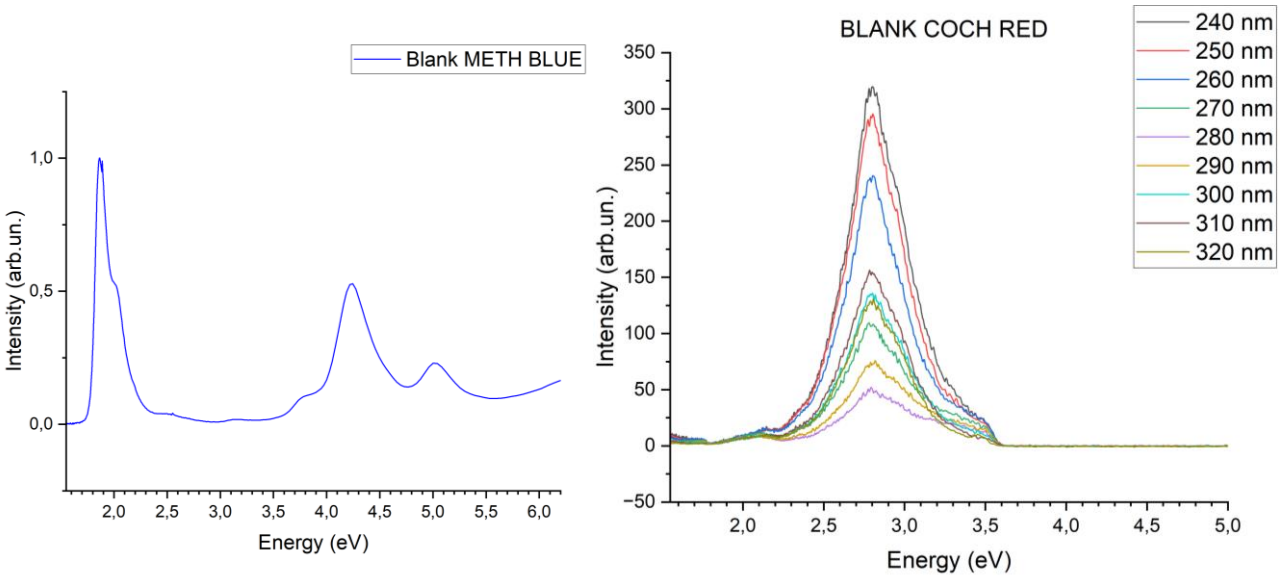

Figure 42. Normalised Methylene Blue (on the left) and non-normalised Cochineal Red (on the right)

Then, it was chosen to report only one sample per type (pristine and dye-conjugated ones), from which a non-normalised and a normalised spectrum was derived. Furthermore, graphs plotting position of the emission peaks against the laser excitation energy are shown.

Starting from the pristine ones, and, in particular, discussing about sample 5, it is possible to spot a peak at lower energy (around 1.76 eV), while other two peaks are at approx. 2.8 eV and 3.51 eV.

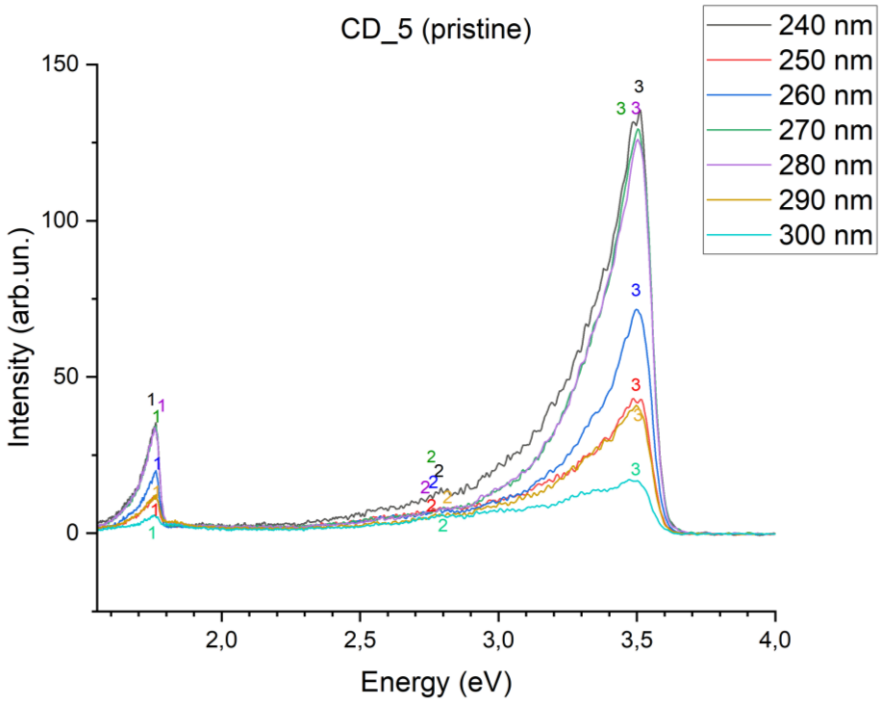

Figure 43. Non-normalised pristine sample 5 emission spectrum.

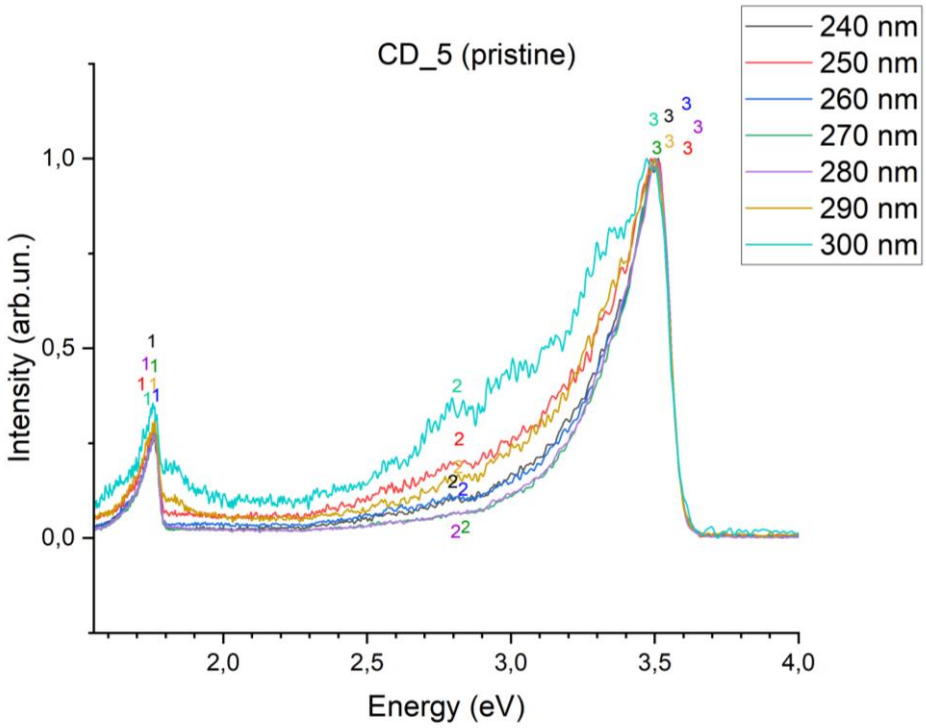

Figure 44. Normalised pristine sample 5 emission spectrum.

In the graph below, showing peak positions on the y-axis against laser energy x-axis, it is possible to appreciate the excitation-independent behaviour of sample 5, which is shared by all the samples.

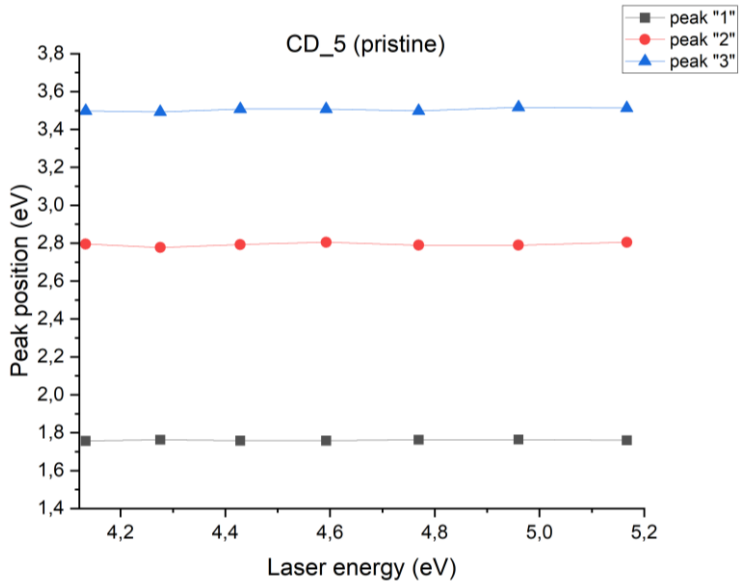

Figure 45. Graph representing excitation-independent behaviour of pristine sample 5.

For what concern MB-conjugated samples, it was decided to display the spectra of sample 2. Visible peaks are approx. at 1.82 eV, 2.6 eV and 3.40 eV. By comparing these spectra with those of pristine ones and those of MB blank in *Figure 42*, a very pronounced emission peak in the red region can be observed. This is an excellent result in terms of the potential photothermal and imaging applications of CDs, as it means that these CDs convert the incident photons less efficiently. In other words, these CDs do not immediately re-emit the incident photon, but, having numerous non-electronic states (vibrational states) that are increased by the introduction of the dye and the extension of the delocalisation it produces over the entire structure, they cause rather efficient non-radiative decays against a less efficient emission (more shifted towards the near-infrared region and therefore less dangerous), as also mentioned in **section 1.2.3.**

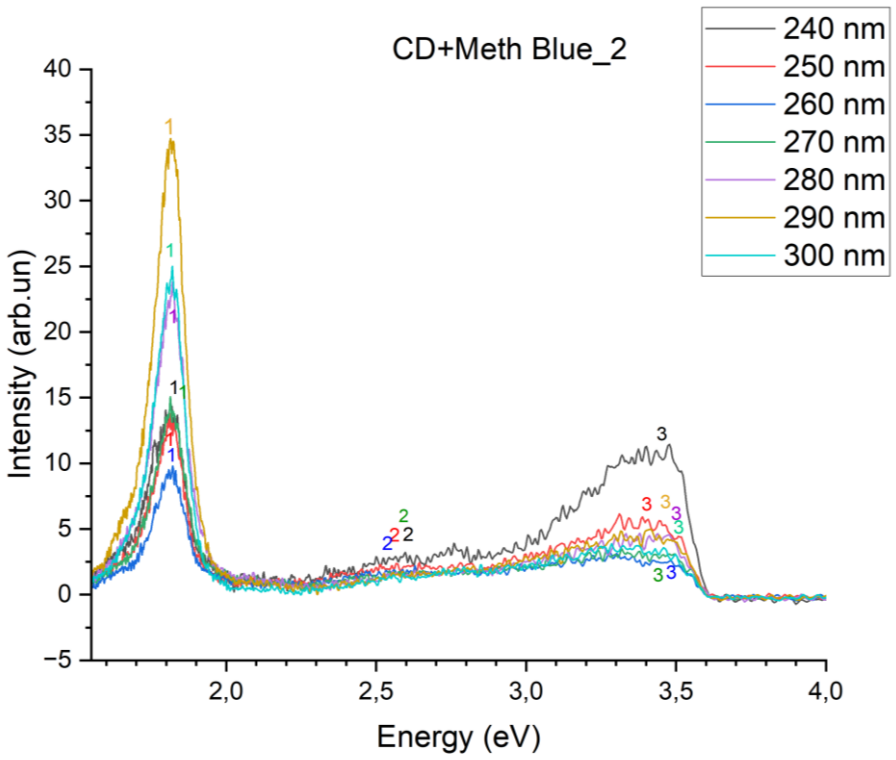

Figure 46. Non-normalised emission spectrum of MB-conjugated sample 2.

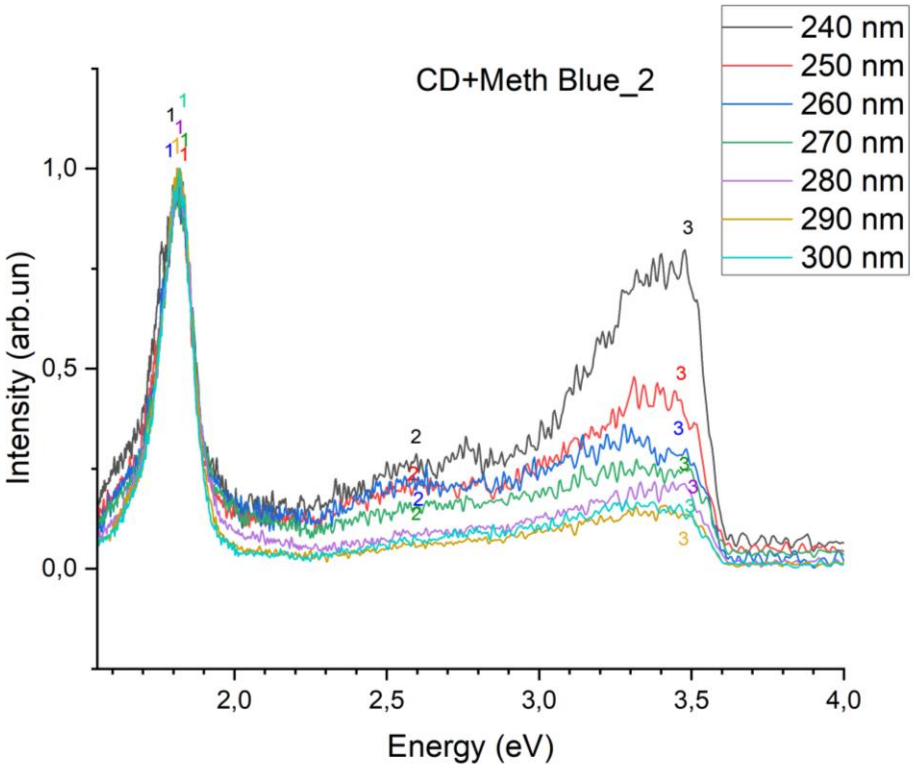

Figure 47. Graph representing excitation-independent behaviour of MB-conjugated sample 2.

Below excitation-independent behaviour of MB-conjugated sample 2 is shown:

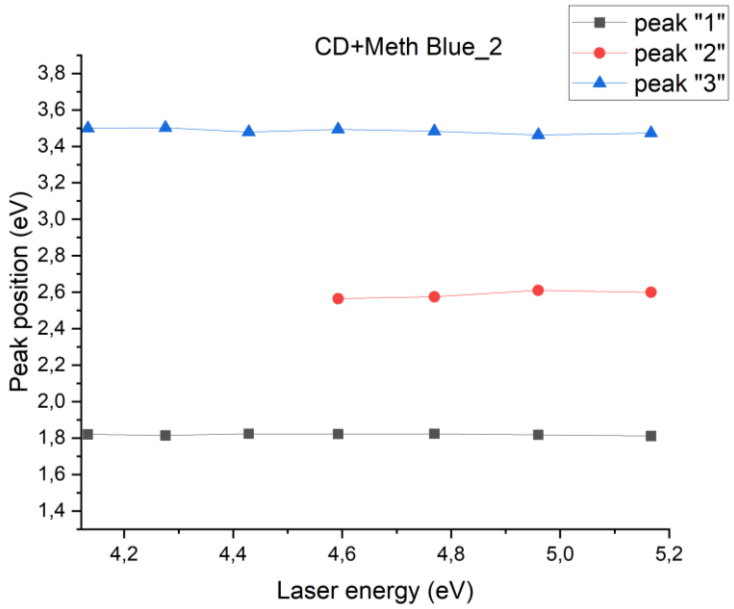

Figure 48. Normalised emission spectrum of MB-conjugated sample 2.

Here, emission spectrum of CR-conjugated sample 3 is shown. It is possible to appreciate a peak at approx. 1.75 eV, a second peak at ca. 2.78 eV and a third one at approximately 3.47 eV.

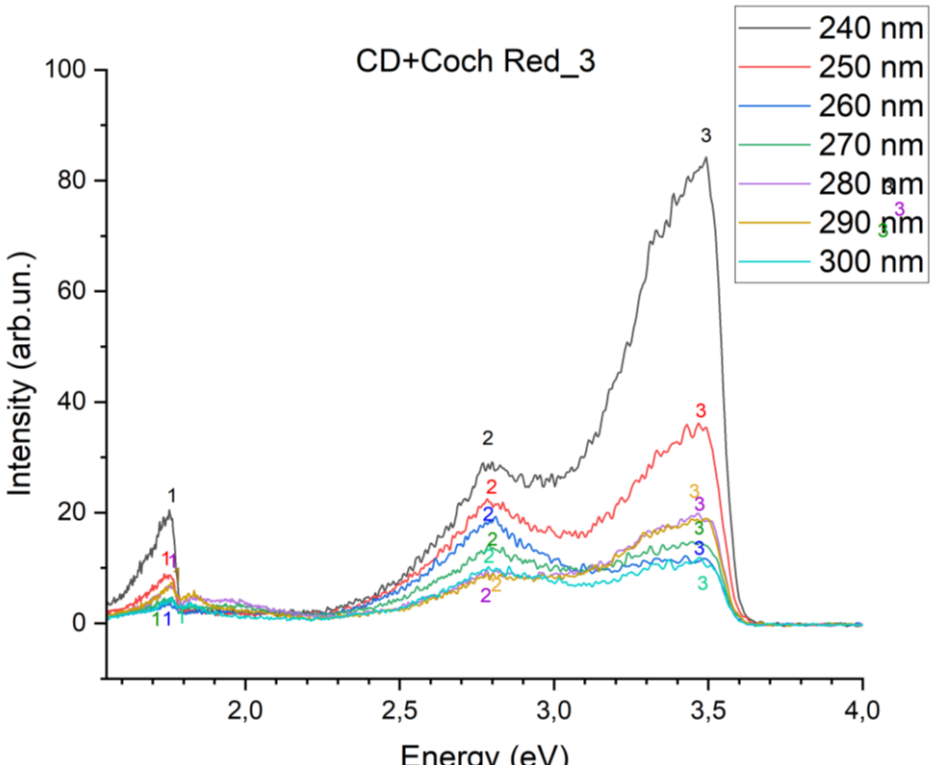

Figure 49. Non-normalised emission spectrum of CR-conjugated sample 3.

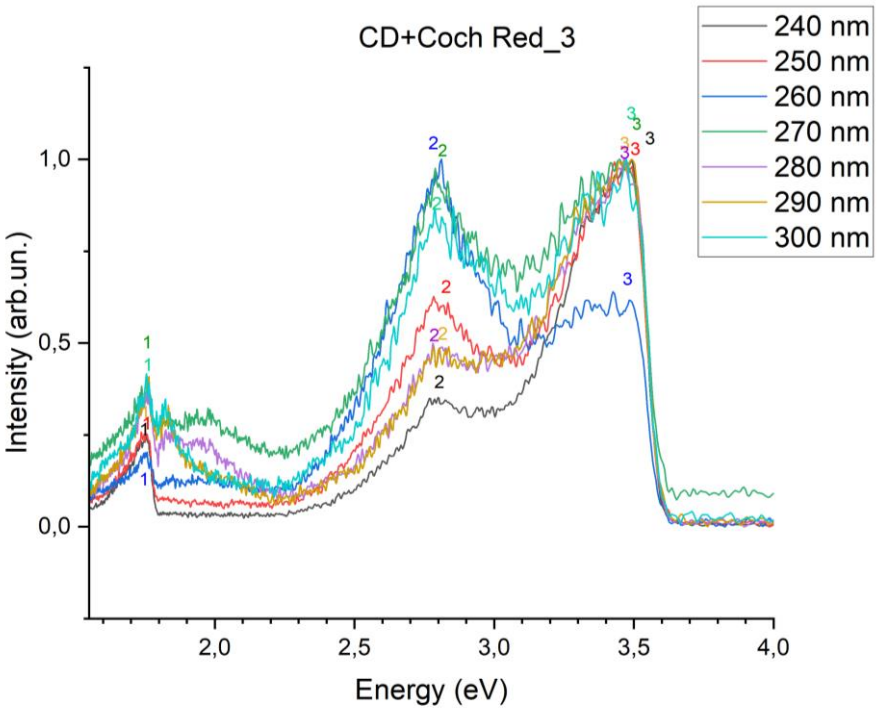

Figure 50. Normalised emission spectrum of CR-conjugated sample 3.

By comparing these spectra with those of pristine samples and of MB-conjugated ones, bearing in mind the Cochineal Red spectrum in *Figure 42* which acts as a blank solution, it is possible to note that the main influence of Cochineal Red is on peaks 2, corresponding to a blue emission, which is a fair result for what concern biomedical applications.

Below, excitation-independent behaviour of CR-conjugated sample 3 can be appreciated.

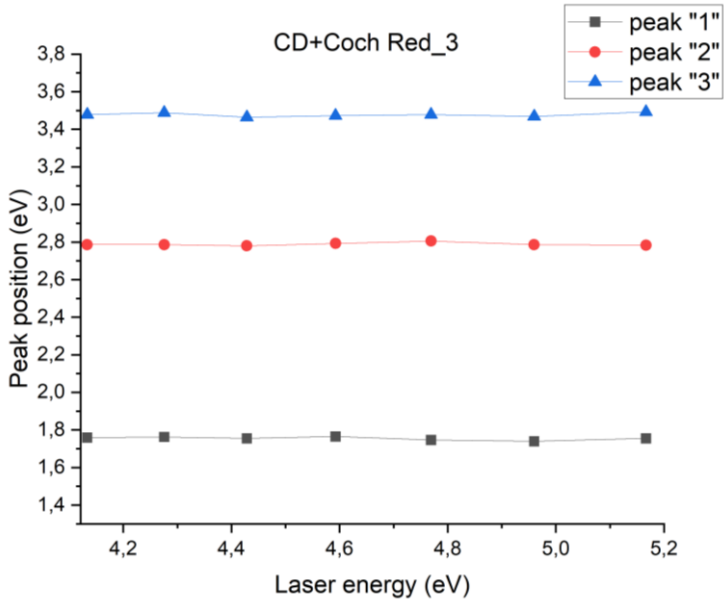

Figure 51. Graph representing excitation-independent behaviour of CR-conjugated sample 3.

As regards σ results of the three samples, here is a table summarizing the width of three bands that can been seen from the emission spectra.

Table 4. σ results of the three samples, indicating the width of three bands visible from the emission spectra.

SPECIES	Bandwidth (eV)	Bandwidth (eV)	Bandwidth (eV)
CD_5	1.245	1.973	2.478
CD+METH BLUE_2	1.285	1.829	2.411
CD+COCH RED_3	0.228	1.975	2.46
	peak "1"	peak "2"	peak "3"

As we can see comparing emission spectra of the three samples and the table, we can note that MB-conjugated samples show an intense and quite wide peak (confirmed by a fairly high σ value vs other samples) due to the presence of a reasonably widespread band throughout the structure thanks to heteroatom doping and its impacts discussed in **section 1.2.4.** Among the other peaks, this one is the most interesting for our discussion of the hypothetical use of carbon dots in teragnostics.

3.5 X-ray Photoelectron Spectroscopy

Through X-Ray photoelectron spectroscopy (XPS), important information could be obtained about the presence of certain elements on the surface of our CDs, particularly carbon, nitrogen and oxygen. being a valid quantitative analysis, the amount of compounds present was also quantified in % by analysing the area under each curve with which the fitting was performed. Below, it is possible to observe the XPS spectra of pristine sample 5. In particular, in *Figure 52 (A)*, which refers to C1s, it is possible to appreciate how the carbon atoms are bonded on the surface, highlighting the various Carbon-containing functional groups. In this case, the carbon hybridized sp^2 is present for the 62 % of the total of the latter, as can be noticed looking at the green curve peaking at 284.5 eV. The following blue curve peaking at 285.7 eV is representative of the C-X moieties (where X= O, N), which account for 33% of the total. Cyan curve representing the C=O moieties is peaked at 287.8 eV and indicates that these functional groups are present for 3% of the total. The last component, the pink one, is assigned to carboxyl groups, whose quantity as a percentage of the total number of carbon functional groups is 2%.

In *Figure 52 (B)* there is the spectrum referring to the oxygen's bounds and functional groups. The first component, the red one, peaking at 531 eV is assigned to hydroxyl groups which are the 12% of the total. Green component, peaking at 532 eV refers to the C=O groups, amounting to 79% of the total. Blue one, peaking at 534 eV, represents carboxyl groups which are the 9% of the total.

Figure 52 (C) shows N-groups, and in particular, it is possible to appreciate a large quantity of amino groups, which amount to 83 % of the total (green component). Red one refers to amides which are the 11% of the total, while blue one is ascribed to pyrrolic N, which are only the 6% of the total.

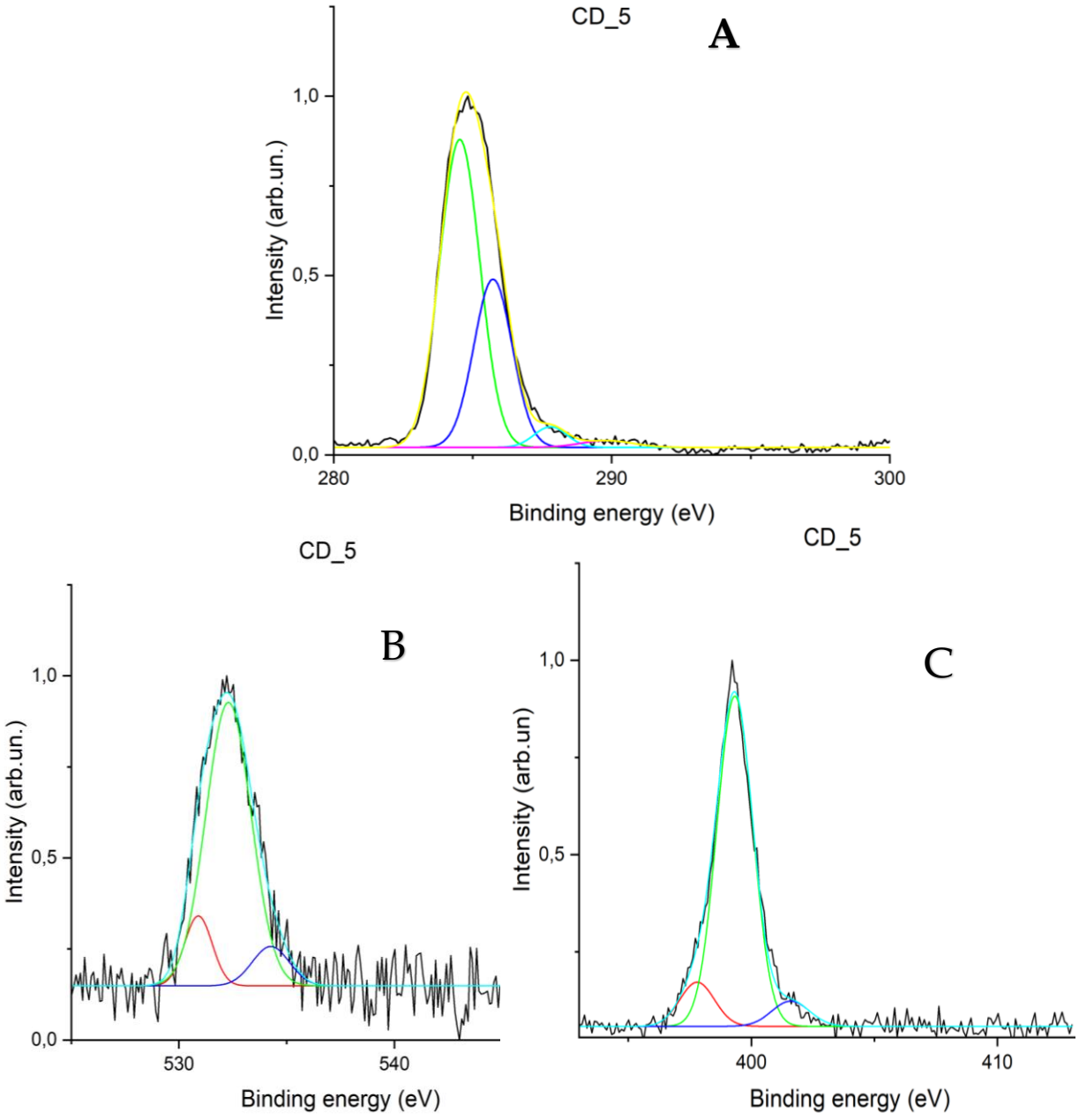

Figure 52. XPS spectra of CD_5. (A) Carbon, (B) Oxygen, (C) Nitrogen.

With regard to MB-conjugated samples, and, in specific, referring to C1s spectrum in *Figure 53 (A)*, carbon hybridized sp^2 are the 58 % of the total of C-containing compounds, while C-X moieties account for 35 % of the total. C=O groups are, instead, only the 7 % of the total and there is no trace of carboxyl groups, which, if present, are in very small quantities.

From O1s spectrum, in *Figure 53 (B)*, it is possible to detect hydroxyl groups (red component) which are the 53 % of the total, while carbonyl groups account for the 47% of the total. The main difference between this sample and pristine one is that here the amount of oxygen groups and, in particular, of the COOH which aren't detected (as well as in the C1s spectrum), is much lower, and this is confirmed by the O1s spectrum that is very noisy. This, probably, is motivated by the fact that Methylene Blue, with its N atoms, introduce more CN single and double bonds, reducing the amount of oxygen groups like COOH, as a result of the formation of amide groups.

Referring to N1s spectrum in *Figure 53 (C)*, it is possible to quantify the amide groups which are the 7% of the total, compared to the amino groups (84%) and pyrrolic N which account for 9% of the total, not deviating too much from the results of the pristine sample, in terms of proportions.

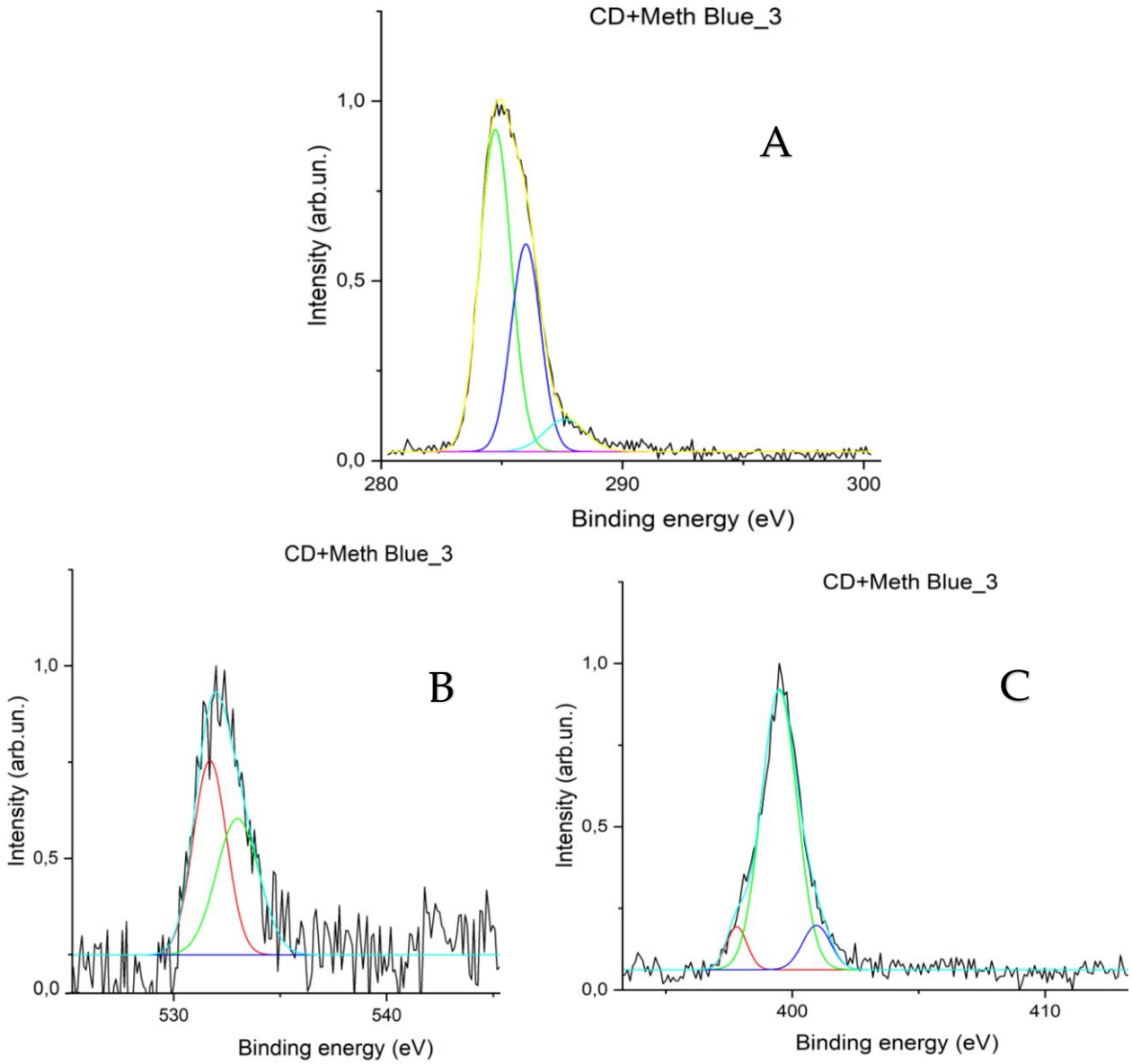

Figure 53. XPS spectra of MB-conjugated sample 3. (A) Carbon, (B) Oxygen, (C) Nitrogen.

Moving to CR-conjugated sample 3, in *Figure 54 (A)* is the spectrum of O1s in which is possible to note, even in this case, a fair quantity of sp^2 carbon compared to the total of oxygen-containing compounds (58%), typical of the aromatic domains (green curve). C-X groups account for 27% of the total. C=O groups are the 8% of the total, while carboxyl groups are present in 15% of the total, a larger quantity compared to other 2 samples.

From O1s spectrum *(Figure 54 (B))*, it is possible to note a huge quantity of OH groups which are the 50% of the total of oxygen-containing compounds (red component). This is probably because of the presence of OH groups in the structure of Cochineal Red. C=O are present for the 39% of the total, while the 11% are carboxyl groups.

From N1s spectrum *(Figure 54 (C))*, it is possible to see that amides make up 60 % of the total of N-containing groups, while amino groups represent the 25% and pyrrolic N the 15% of the total. Hence, it is possible to justify these results, considering the large amount of OH, carbonyl and carboxyl groups in the structure of Cochineal Red which can react with NH_2 groups of p-DPA giving rise to more amides.

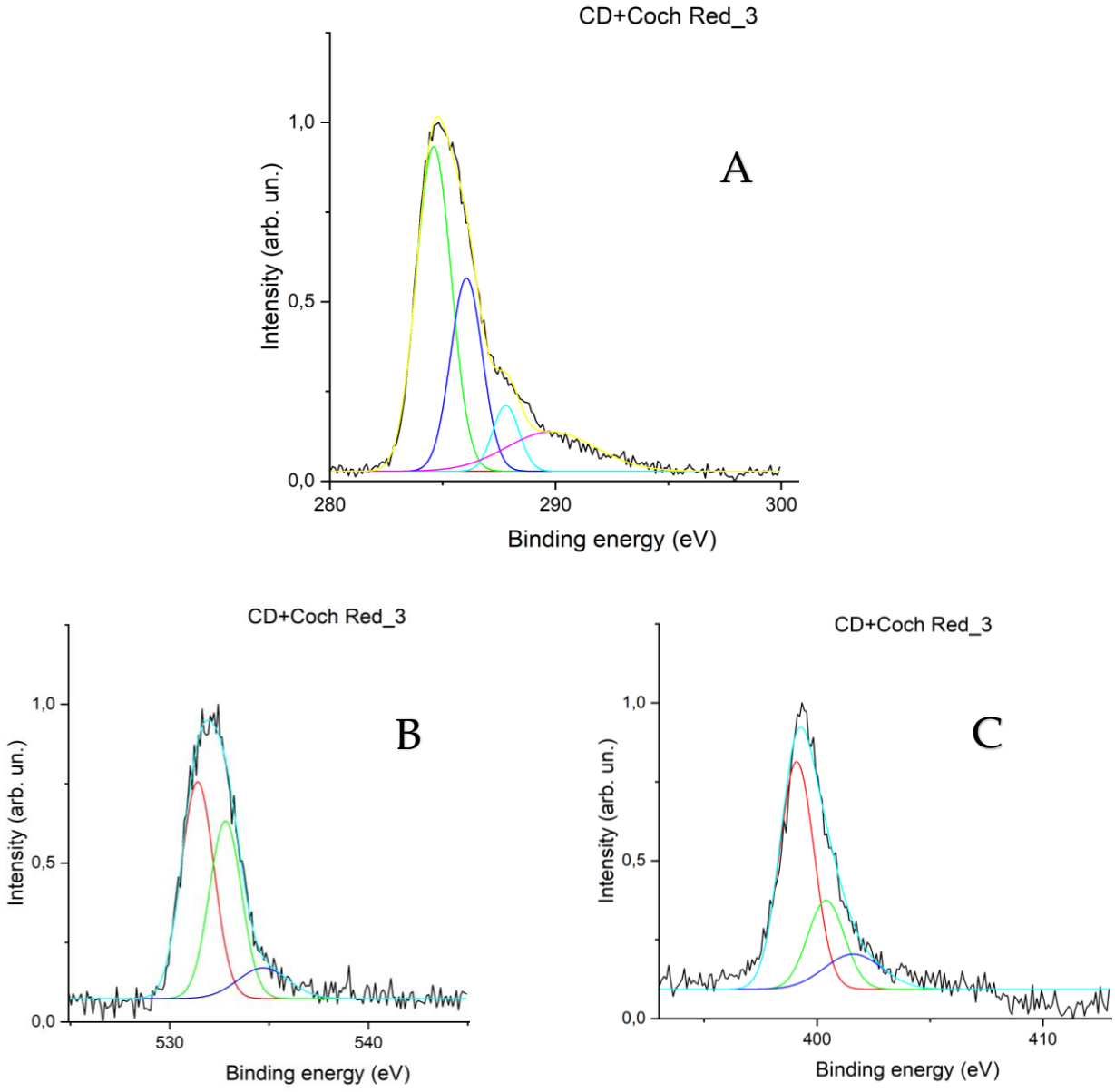

Figure 54. XPS spectra of CR-conjugated sample 3. (A) Carbon, (B) Oxygen, (C) Nitrogen.

3.6 Radical scavenging results

Regarding the evaluation of radical scavenging activity, first of all graphs illustrating absorbance of Curcumin alone (at different concentrations), before and after irradiation, are shown above, from which a significant degradation of irradiated curcumin alone can be perceived.

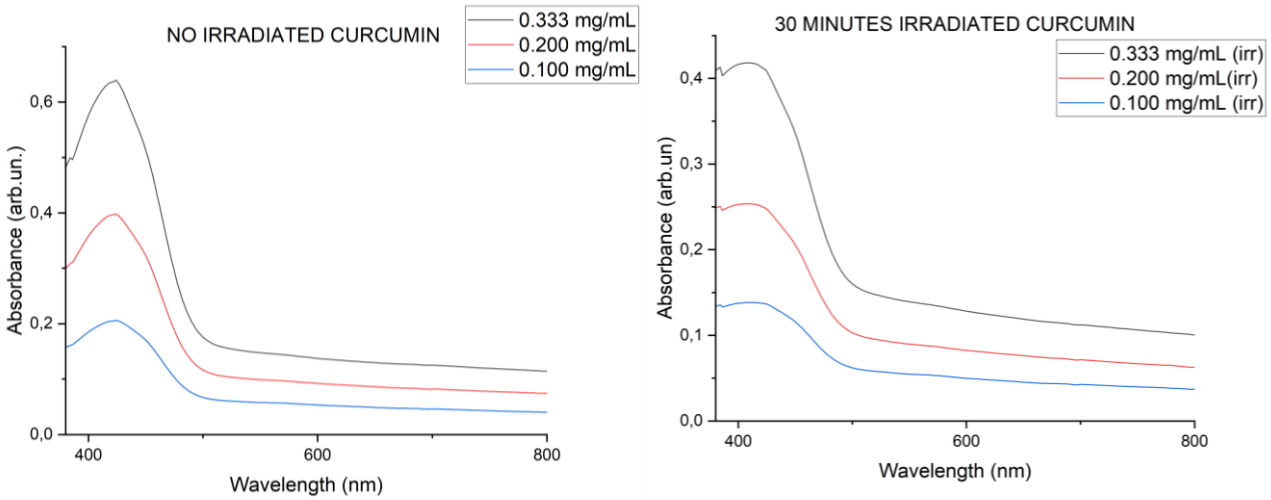

Figure 55. Curcumin in solution with water without CDs before (to the left) and after 30 minutes of irradiation (to the right).

Then, following graphs show results from irradiation of three CDs solutions (one for each type, pristine and dye-conjugated samples at different concentrations) with Curcumin, and a less degradation of the latter can be appreciated. Hence, it's possible to confirm the antioxidant capacity of CDs envisaged **in chapter 2.**

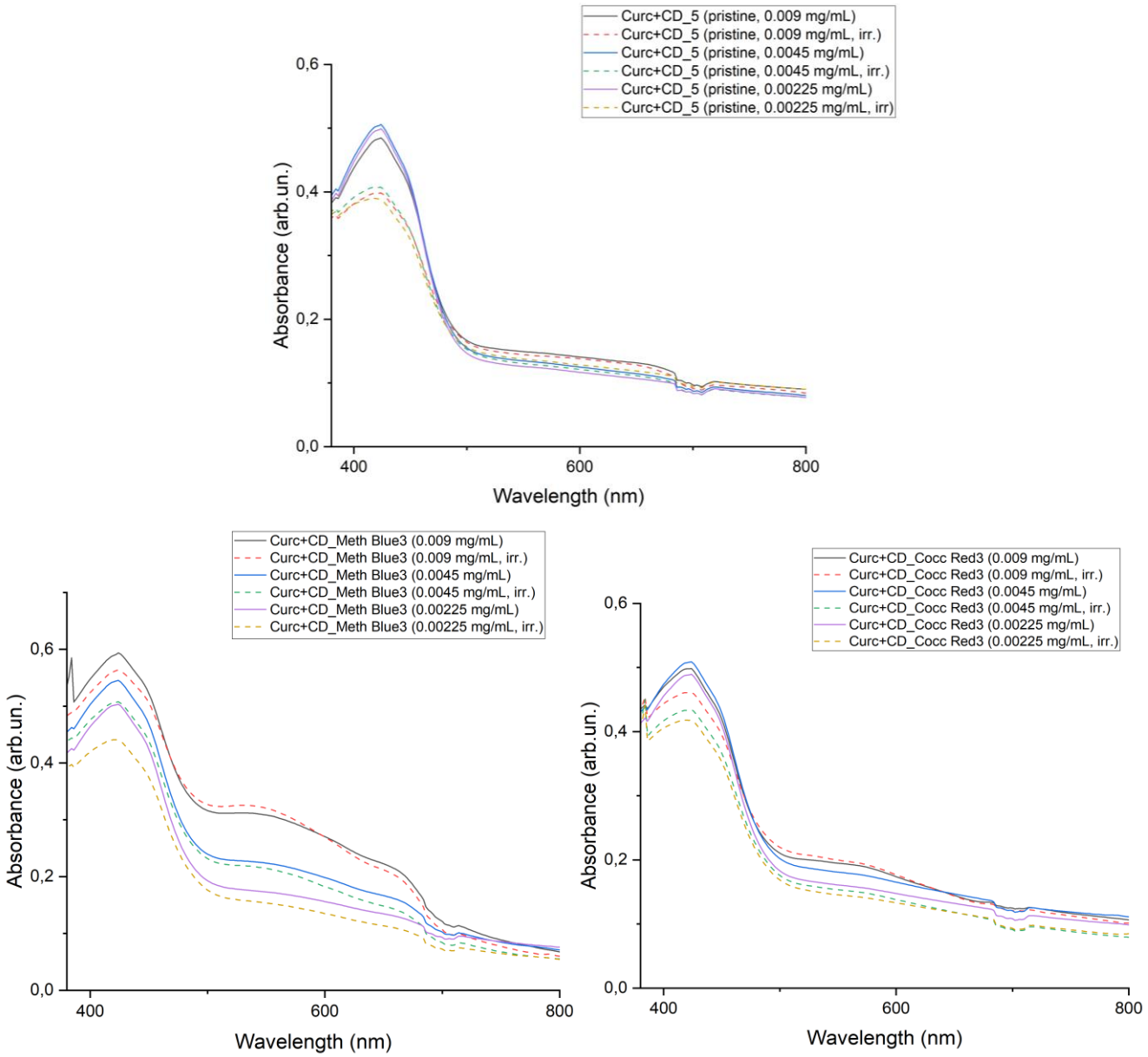

Figure 56. Graphs representing three solutions for each type of CDs with curcumin, before and after irradiation.

Finally, here is a table summarizing the results in terms of degradation of Curcumin and its prevention permitted by the presence of each of the three types of CD, for which an average has been calculated. Outcomes show better performance in radical scavenging by those conjugated with Methylene Blue, and this, together with the results obtained from the fluorometer, confirms what was defined to be the purpose of this thesis.

Table 5. Results of the scavenging activity of the three types of CDs.

SPECIES	DEGRADATION %	PREVENTION %	DEGRADATION %	PREVENTION %	DEGRADATION %	PREVENTION %
CURCUMA ALONE	100	0				
CURCUMA + PRISTINE CDs	40.2	59.8	54.5	45.5	61.2	38.8
CURCUMA + MET BLUE_TOT	23.3	76.7	29.3	70.7	34.6	65.4
CURCUMA + COCH RED_TOT	29.2	70.8	41	59	40.4	59.6
	0.009 mg/mL		0.0045 mg/mL		0.00225 mg/mL	

CHAPTER 4 CONCLUSIONS

In this thesis, the topics of synthesising Carbon Dots to modify their absorption and emission properties by adding two dyes, Methylene Blue and Cochineal Red, during synthesis were addressed, all to make the radical scavenging process more effective, which is one of the applications in which Carbon Dots have proved to be successful. This has been observed through a process induced by UV irradiation on a reactive molecule, Curcumin, which is sensitive to oxidative stress. Results showed that Methylene Blue proved to be the best solution among those tested for reducing oxidative stress, preventing Curcumin degradation more efficiently.

Furthermore, it was noted through fluorometric analysis that Methylene Blue samples are more suitable in a probable and desirable use in the field of photothermal therapy and real time in vivo imaging, being able to emit more in the NIR region, which is the best for obtaining a correct photothermal effect and good tissue penetration (in vivo imaging). Fair results were obtained also with Cochineal Red, suggesting that dye addiction to pristine CDs is generally a good solution for the abovementioned purposes. This can be explained considering the importance, demonstrated also by various works in literature, of heteroatom doping, in this case induced by dye's atoms and functional groups, which leads to an increase in non-electronic states with a consequent decrease in bandgap and red-shift emissions.

All Carbon Dots were also characterised by UV/VIS to evaluate their absorbance and to see whether or not the dyes had bonded. Then, a qualitative analysis of the functional groups present in the structure was performed using the FT-IR spectrometer, while a quantitative one was obtained through XPS. They were both consistent with the proposed growth mechanism and the hypothesised structural model.

Future developments of this technology may include improvements in the efficiency of reaction yields and a more detailed analysis of the bandgap and the possibility/manner of modifying it. They may also include more investigations as those obtainable through thermogravimetric analysis to evaluate Carbon Dots temperature-dependent degradation and microscopic analysis to examine the morphology and dispersion of the prepared CDs.

CHAPTER 5 ACKNOWLEDGEMENTS

Foremost, I would like to acknowledge Professor Tagliaferro for giving me the opportunity to work on this exciting project and allowing me to join his research group. In particular, I am sincerely grateful to my supervisor Mattia Bartoli for his invaluable advice on the research subject and his continuous support and patience that guided me through this research. I would also like to take this opportunity to express my gratitude to all those people of the research group who have given their valuable assistance and suggestions throughout these months in the laboratory. I wish you all the best for your future and that you achieve all your goals.

It is impossible to extend enough thanks to all my family members. Each one of you has given me so much in terms of affection, teachings and encouragement over all these years. Especially, I would like to thank my parents who gave me the possibility to live this incredible experience. They allowed me to take opportunities that challenged me and helped to grow personally during these years.

A special mention goes to Claudia. I can't thank you enough for the way you have always supported me and believed in me more than I did. The way you enrich my days with your energy and affection is something priceless. You're unique and I am so lucky to have you by my side.

Then, I would like to thank my friends from the university who have accompanied me during these years (both in Turin and Palermo) and with whom I have shared beautiful moments and experiences. You have proven yourself to be truly genuine friends who I can count on.

Last, but definitely not the least, to all my long-term friends from Palermo who have been supporting me despite the distance and with whom I have shared some of the happiest moments in my life.

REFERENCES

[1] J. Wang, N. Liu, H. Jiang, Q. Li, and D. Xing, "Reactive Oxygen Species in Anticancer Immunity: A Double-Edged Sword," *Front. Bioeng. Biotechnol.*, vol. 9, Nov. 2021, doi: 10.3389/fbioe.2021.784612.

[2] M. Schieber and N. S. Chandel, "ROS Function in Redox Signaling and Oxidative Stress," *Curr. Biol.*, vol. 24, no. 10, pp. R453–R462, May 2014, doi: 10.1016/j.cub.2014.03.034.

[3] P. C. P. Watts, P. K. Fearon, W. K. Hsu, N. C. Billingham, H. W. Kroto, and D. R. M. Walton, "Carbon nanotubes as polymer antioxidants," *J. Mater. Chem.*, vol. 13, no. 3, pp. 491–495, Feb. 2003, doi: 10.1039/b211328g.

[4] M. Antolovich, P. D. Prenzler, E. Patsalides, S. McDonald, and K. Robards, "Methods for testing antioxidant activity," *Analyst*, vol. 127, no. 1, pp. 183–198, Jan. 2002, doi: 10.1039/b009171p.

[5] H. Ohshima, Y. Yoshie, S. Auriol, and I. Gilibert, "Antioxidant and pro-oxidant actions of flavonoids: effects on DNA damage induced by nitric oxide, peroxynitrite and nitroxyl anion," *Free Radic. Biol. Med.*, vol. 25, no. 9, pp. 1057–1065, Dec. 1998, doi: 10.1016/S0891-5849(98)00141-5.

[6] Q. Li, X. Shen, and D. Xing, "Carbon quantum dots as ROS-generator and -scavenger: A comprehensive review," *Dye. Pigment.*, vol. 208, p. 110784, Dec. 2022, doi: 10.1016/j.dyepig.2022.110784.

[7] S. B. Nimse and D. Pal, "Free radicals, natural antioxidants, and their reaction mechanisms," *RSC Adv.*, vol. 5, no. 35, pp. 27986–28006, Mar. 2015, doi: 10.1039/C4RA13315C.

[8] K. Jakubczyk, K. Dec, J. Kałduńska, D. Kawczuga, J. Kochman, and K. Janda, "Reactive oxygen species - sources, functions, oxidative damage.," *Pol. Merkur. Lekarski*, vol. 48, no. 284, pp. 124–127, Apr. 2020, [Online]. Available: http://www.ncbi.nlm.nih.gov/pubmed/32352946.

[9] D. M. Arvapalli, A. T. Sheardy, J. J. Bang, and J. Wei, "Antiproliferative and ROS Regulation Activity of Photoluminescent Curcumin-Derived Nanodots," *ACS Appl. Bio Mater.*, vol. 4, no. 12, pp. 8477–8486, 2021, doi: 10.1021/acsabm.1c00991.

[10] P. Jenner, "Oxidative stress in Parkinson's disease," *Ann. Neurol.*, vol. 53, no. S3, pp. S26–S38, 2003, doi: 10.1002/ana.10483.

[11] S. A. A. Comhair *et al.*, "Correlation of Systemic Superoxide Dismutase Deficiency to Airflow Obstruction in Asthma," *Am. J. Respir. Crit. Care Med.*, vol. 172, no. 3, pp. 306–313, Aug. 2005, doi: 10.1164/rccm.200502-180OC.

[12] E. Birben, U. M. Sahiner, C. Sackesen, S. Erzurum, and O. Kalayci, "Oxidative Stress and Antioxidant Defense," *World Allergy Organ. J.*, vol. 5, no. 1, pp. 9–19, 2012, doi: 10.1097/WOX.0b013e3182439613.

[13] H. Wang *et al.*, "Carbon Dots Derived from Citric Acid and Glutathione as a Highly Efficient Intracellular Reactive Oxygen Species Scavenger for Alleviating the Lipopolysaccharide-

Induced Inflammation in Macrophages," *ACS Appl. Mater. Interfaces*, vol. 12, no. 37, pp. 41088–41095, 2020, doi: 10.1021/acsami.0c11735.

[14] M. Alfonso-Prieto, X. Biarnés, P. Vidossich, and C. Rovira, "The molecular mechanism of the catalase reaction," *J. Am. Chem. Soc.*, vol. 131, no. 33, pp. 11751–11761, Aug. 2009, doi: 10.1021/JA9018572/SUPPL_FILE/JA9018572_SI_001.PDF.

[15] M. Doseděl *et al.*, "Vitamin C-Sources, Physiological Role, Kinetics, Deficiency, Use, Toxicity, and Determination," *Nutrients*, vol. 13, no. 2, pp. 1–36, Feb. 2021, doi: 10.3390/NU13020615.

[16] R. C. Rose and A. M. Bode, "Biology of free radical scavengers: an evaluation of ascorbate," *FASEB J.*, vol. 7, no. 12, pp. 1135–1142, Sep. 1993, doi: 10.1096/fasebj.7.12.8375611.

[17] X. Li, T. Chen, L. Xu, Z. Zhang, L. Li, and H. Chen, "Preparation of curcumin micelles and the in vitro and in vivo evaluation for cancer therapy," *J. Biomed. Nanotechnol.*, vol. 10, no. 8, pp. 1458–1468, 2014, doi: 10.1166/JBN.2014.1840.

[18] I. Rahman, S. K. Biswas, and P. A. Kirkham, "Regulation of inflammation and redox signaling by dietary polyphenols," *Biochem. Pharmacol.*, vol. 72, no. 11, pp. 1439–1452, Nov. 2006, doi: 10.1016/J.BCP.2006.07.004.

[19] K. Dehvari, S. H. Chiu, J. S. Lin, W. M. Girma, Y. C. Ling, and J. Y. Chang, "Heteroatom doped carbon dots with nanoenzyme like properties as theranostic platforms for free radical scavenging, imaging, and chemotherapy," *Acta Biomater.*, vol. 114, pp. 343–357, 2020, doi: 10.1016/j.actbio.2020.07.022.

[20] P. Innocenzi and L. Stagi, "Carbon dots as oxidant-antioxidant nanomaterials, understanding the structure-properties relationship. A critical review," *Nano Today*, vol. 50, p. 101837, Jun. 2023, doi: 10.1016/j.nantod.2023.101837.

[21] J. Zhou *et al.*, "Mechanisms and Kinetics Studies of Butylated Hydroxytoluene Degradation to Isobutene," *J. Phys. Chem. A*, vol. 2022, pp. 3210–3218, 2022, doi: 10.1021/acs.jpca.2c01961.

[22] W. A. Yehye *et al.*, "Understanding the chemistry behind the antioxidant activities of butylated hydroxytoluene (BHT): A review," *Eur. J. Med. Chem.*, vol. 101, pp. 295–312, Aug. 2015, doi: 10.1016/j.ejmech.2015.06.026.

[23] H. P. Witschi, "Enhanced tumour development by butylated hydroxytoluene (BHT) in the liver, lung and gastro-intestinal tract," *Food Chem. Toxicol.*, vol. 24, no. 10–11, pp. 1127–1130, Oct. 1986, doi: 10.1016/0278-6915(86)90298-X.

[24] B. Dassarma, D. K. Nandi, S. Gangopadhyay, and S. Samanta, "Hepatoprotective effect of food preservatives (butylated hydroxyanisole, butylated hydroxytoluene) on carbon tetrachloride-induced hepatotoxicity in rat," *Toxicol. Reports*, vol. 5, pp. 31–37, 2018, doi: 10.1016/j.toxrep.2017.12.009.

[25] R. Kahl and H. Kappus, "[Toxicology of the synthetic antioxidants BHA and BHT in comparison with the natural antioxidant vitamin E].," *Z. Lebensm. Unters. Forsch.*, vol. 196, no. 4, pp. 329–338, Apr. 1993, doi: 10.1007/BF01197931.

[26] K. J. Mintz *et al.*, "Tryptophan carbon dots and their ability to cross the blood-brain barrier," *Colloids Surfaces B Biointerfaces*, vol. 176, pp. 488–493, Apr. 2019, doi:

10.1016/j.colsurfb.2019.01.031.

[27] E. Kirbas Cilingir *et al.*, "Surface modification of carbon nitride dots by nanoarchitectonics for better drug loading and higher cancer selectivity," *Nanoscale*, vol. 14, no. 27, pp. 9686–9701, 2022, doi: 10.1039/d2nr02063g.

[28] G. Getachew, C. Korupalli, A. S. Rasal, and J.-Y. Chang, "ROS generation/scavenging modulation of carbon dots as phototherapeutic candidates and peroxidase mimetics to integrate with polydopamine nanoparticles/GOx towards cooperative cancer therapy," *Compos. Part B Eng.*, vol. 226, p. 109364, Dec. 2021, doi: 10.1016/j.compositesb.2021.109364.

[29] Z. Zhang *et al.*, "A minireview on doped carbon dots for photocatalytic and electrocatalytic applications," *Nanoscale*, vol. 12, no. 26, pp. 13899–13906, 2020, doi: 10.1039/D0NR03163A.

[30] W. Pang *et al.*, "Nucleolus-Targeted Photodynamic Anticancer Therapy Using Renal-Clearable Carbon Dots," *Adv. Healthc. Mater.*, vol. 9, no. 16, p. 2000607, Aug. 2020, doi: 10.1002/adhm.202000607.

[31] J. Chen *et al.*, "Graphene quantum dots in photodynamic therapy," *Nanoscale Adv.*, vol. 2, no. 10, pp. 4961–4967, 2020, doi: 10.1039/D0NA00631A.

[32] S. Zhao *et al.*, "Lysosome-targetable carbon dots for highly efficient photothermal/photodynamic synergistic cancer therapy and photoacoustic/two-photon excited fluorescence imaging," *Chem. Eng. J.*, vol. 388, p. 124212, May 2020, doi: 10.1016/j.cej.2020.124212.

[33] D.-K. Ji *et al.*, "Controlled functionalization of carbon nanodots for targeted intracellular production of reactive oxygen species," *Nanoscale Horizons*, vol. 5, no. 8, pp. 1240–1249, 2020, doi: 10.1039/D0NH00300J.

[34] Q. Jia *et al.*, "A Magnetofluorescent Carbon Dot Assembly as an Acidic H 2 O 2 -Driven Oxygenerator to Regulate Tumor Hypoxia for Simultaneous Bimodal Imaging and Enhanced Photodynamic Therapy," *Adv. Mater.*, vol. 30, no. 13, p. 1706090, Mar. 2018, doi: 10.1002/adma.201706090.

[35] M. Lan *et al.*, "Carbon Dots as Multifunctional Phototheranostic Agents for Photoacoustic/Fluorescence Imaging and Photothermal/Photodynamic Synergistic Cancer Therapy," *Adv. Ther.*, vol. 1, no. 6, p. 1800077, Oct. 2018, doi: 10.1002/adtp.201800077.

[36] T. C. Wareing, P. Gentile, and A. N. Phan, "Biomass-Based Carbon Dots: Current Development and Future Perspectives," *ACS Nano*, vol. 15, no. 10, pp. 15471–15501, Oct. 2021, doi: 10.1021/acsnano.1c03886.

[37] P. Zuo, X. Lu, Z. Sun, Y. Guo, and H. He, "A review on syntheses, properties, characterization and bioanalytical applications of fluorescent carbon dots," *Microchim. Acta*, vol. 183, no. 2, pp. 519–542, Feb. 2016, doi: 10.1007/s00604-015-1705-3.

[38] B. Das, P. Pal, P. Dadhich, J. Dutta, and S. Dhara, "In Vivo Cell Tracking, Reactive Oxygen Species Scavenging, and Antioxidative Gene Down Regulation by Long-Term Exposure of Biomass-Derived Carbon Dots," *ACS Biomater. Sci. Eng.*, vol. 5, no. 1, pp. 346–356, 2019, doi: 10.1021/acsbiomaterials.8b01101.

[39] J. Ge *et al.*, "Carbon Dots with Intrinsic Theranostic Properties for Bioimaging, Red-Light-

Triggered Photodynamic/Photothermal Simultaneous Therapy In Vitro and In Vivo," *Adv. Healthc. Mater.*, vol. 5, no. 6, pp. 665–675, 2016, doi: 10.1002/adhm.201500720.

[40] F. A. Vallejo, G. Sigdel, E. A. Veliz, R. M. Leblanc, S. Vanni, and R. M. Graham, "Carbon Dots in Treatment of Pediatric Brain Tumors : Past , Present , and Future Directions," 2023.

[41] D. O. Lopez-Cantu *et al.*, "Enzyme-mimicking capacities of carbon-dots nanozymes: Properties, catalytic mechanism, and applications – A review," *Int. J. Biol. Macromol.*, vol. 194, pp. 676–687, Jan. 2022, doi: 10.1016/j.ijbiomac.2021.11.112.

[42] D. B. Gunjal *et al.*, "Nitrogen doped waste tea residue derived carbon dots for selective quantification of tetracycline in urine and pharmaceutical samples and yeast cell imaging application," *Opt. Mater. (Amst).*, vol. 98, p. 109484, Dec. 2019, doi: 10.1016/J.OPTMAT.2019.109484.

[43] Y. Zhou *et al.*, "Multicolor carbon nanodots from food waste and their heavy metal ion detection application," *RSC Adv.*, vol. 8, no. 42, pp. 23657–23662, Jun. 2018, doi: 10.1039/C8RA03272F.

[44] A. Prasannan and T. Imae, "One-Pot Synthesis of Fluorescent Carbon Dots from Orange Waste Peels," *Ind. Eng. Chem. Res.*, vol. 52, no. 44, pp. 15673–15678, Nov. 2013, doi: 10.1021/ie402421s.

[45] L. Wang *et al.*, "Facile synthesis of fluorescent graphene quantum dots from coffee grounds for bioimaging and sensing," *Chem. Eng. J.*, vol. 300, pp. 75–82, Sep. 2016, doi: 10.1016/j.cej.2016.04.123.

[46] H. Miao, Y. Wang, and X. Yang, "Carbon dots derived from tobacco for visually distinguishing and detecting three kinds of tetracyclines," *Nanoscale*, vol. 10, no. 17, pp. 8139–8145, May 2018, doi: 10.1039/C8NR02405G.

[47] S. Zhao *et al.*, "Green Synthesis of Bifunctional Fluorescent Carbon Dots from Garlic for Cellular Imaging and Free Radical Scavenging," *ACS Appl. Mater. Interfaces*, vol. 7, no. 31, pp. 17054–17060, 2015, doi: 10.1021/acsami.5b03228.

[48] M. Lan *et al.*, "Carbon Dots as Multifunctional Phototheranostic Agents for Photoacoustic/Fluorescence Imaging and Photothermal/Photodynamic Synergistic Cancer Therapy," *Adv. Ther.*, vol. 1, no. 6, p. 1800077, Oct. 2018, doi: 10.1002/ADTP.201800077.

[49] C. Xia *et al.*, "Evolution and Synthesis of Carbon Dots: From Carbon Dots to Carbonized Polymer Dots," *Adv. Sci.*, vol. 6, no. 23, p. 1901316, Dec. 2019, doi: 10.1002/ADVS.201901316.

[50] S. Zhou, Y. Sui, X. Zhu, X. Sun, S. Zhuo, and H. Li, "Study and Comparison on Purification Methods of Multicolor Emission Carbon Dots," *Chem. Asian J.*, vol. 16, no. 4, pp. 348–354, Feb. 2021, doi: 10.1002/ASIA.202001352.

[51] Y. Zhou *et al.*, "Photoluminescent Carbon Dots: A Mixture of Heterogeneous Fractions," *ChemPhysChem*, vol. 19, no. 19, pp. 2589–2597, Oct. 2018, doi: 10.1002/cphc.201800248.

[52] C. Kang, Y. Huang, H. Yang, X. F. Yan, and Z. P. Chen, "A review of carbon dots produced from biomass wastes," *Nanomaterials*, vol. 10, no. 11, pp. 1–24, 2020, doi: 10.3390/nano10112316.

[53] S. Zhu, Y. Song, X. Zhao, J. Shao, J. Zhang, and B. Yang, "The photoluminescence

mechanism in carbon dots (graphene quantum dots, carbon nanodots, and polymer dots): current state and future perspective," *Nano Res.*, vol. 8, no. 2, pp. 355–381, Feb. 2015, doi: 10.1007/s12274-014-0644-3.

[54] X. Miao *et al.*, "Synthesis of Carbon Dots with Multiple Color Emission by Controlled Graphitization and Surface Functionalization," *Adv. Mater.*, vol. 30, no. 1, p. 1704740, Jan. 2018, doi: 10.1002/ADMA.201704740.

[55] K. Zheng *et al.*, "Controllable synthesis highly efficient red, yellow and blue carbon nanodots for photo-luminescent light-emitting devices," *Chem. Eng. J.*, vol. 380, p. 122503, Jan. 2020, doi: 10.1016/J.CEJ.2019.122503.

[56] C. Xia *et al.*, "Hydrothermal Addition Polymerization for Ultrahigh-Yield Carbonized Polymer Dots with Room Temperature Phosphorescence via Nanocomposite," *Chem. – A Eur. J.*, vol. 24, no. 44, pp. 11303–11308, Aug. 2018, doi: 10.1002/CHEM.201802712.

[57] S. Tao, Y. Song, S. Zhu, J. Shao, and B. Yang, "A new type of polymer carbon dots with high quantum yield: From synthesis to investigation on fluorescence mechanism," *Polymer (Guildf).*, vol. 116, pp. 472–478, May 2017, doi: 10.1016/J.POLYMER.2017.02.039.

[58] S. K. Bhunia, A. Saha, A. R. Maity, S. C. Ray, and N. R. Jana, "Carbon nanoparticle-based fluorescent bioimaging probes," *Sci. Rep.*, vol. 3, 2013, doi: 10.1038/SREP01473.

[59] H. Liu, T. Ye, and C. Mao, "Fluorescent carbon nanoparticles derived from candle soot," *Angew. Chem. Int. Ed. Engl.*, vol. 46, no. 34, pp. 6473–6475, 2007, doi: 10.1002/ANIE.200701271.

[60] H. Li *et al.*, "Water-soluble fluorescent carbon quantum dots and photocatalyst design," *Angew. Chem. Int. Ed. Engl.*, vol. 49, no. 26, pp. 4430–4434, Jun. 2010, doi: 10.1002/ANIE.200906154.

[61] S. Zhu *et al.*, "The crosslink enhanced emission (CEE) in non-conjugated polymer dots: from the photoluminescence mechanism to the cellular uptake mechanism and internalization," *Chem. Commun.*, vol. 50, no. 89, pp. 13845–13848, Oct. 2014, doi: 10.1039/C4CC05806B.

[62] A. Stergiou and N. Tagmatarchis, "Interfacing Carbon Dots for Charge-Transfer Processes," *Small*, vol. 17, no. 48, pp. 1–10, 2021, doi: 10.1002/smll.202006005.

[63] M. J. Molaei, "Principles, mechanisms, and application of carbon quantum dots in sensors: A review," *Anal. Methods*, vol. 12, no. 10, pp. 1266–1287, 2020, doi: 10.1039/c9ay02696g.

[64] M. G. Giordano, G. Seganti, and M. Bartoli, "Chemical Features," 2023.

[65] S. Y. Li and L. He, "Recent progresses of quantum confinement in graphene quantum dots," *Front. Phys. 2022 173*, vol. 17, no. 3, pp. 1–25, Nov. 2021, doi: 10.1007/S11467-021-1125-2.

[66] H. Liu, J. Ding, K. Zhang, and L. Ding, "Construction of biomass carbon dots based fluorescence sensors and their applications in chemical and biological analysis," *TrAC Trends Anal. Chem.*, vol. 118, pp. 315–337, Sep. 2019, doi: 10.1016/J.TRAC.2019.05.051.

[67] M. T. Dejpasand, E. Saievar-Iranizad, A. Bayat, A. Montaghemi, and S. R. Ardekani, "Tuning HOMO and LUMO of three region (UV, Vis and IR) photoluminescent nitrogen doped graphene quantum dots for photodegradation of methylene blue," *Mater. Res. Bull.*, vol. 128, no. February, p. 110886, 2020, doi: 10.1016/j.materresbull.2020.110886.

[68] M. A. Sk, A. Ananthanarayanan, L. Huang, K. H. Lim, and P. Chen, "Revealing the tunable photoluminescence properties of graphene quantum dots," *J. Mater. Chem. C*, vol. 2, no. 34, pp. 6954–6960, Aug. 2014, doi: 10.1039/C4TC01191K.

[69] J. Du *et al.*, "Insight into the effect of functional groups on visible-fluorescence emissions of graphene quantum dots," *J. Mater. Chem. C*, vol. 4, no. 11, pp. 2235–2242, Mar. 2016, doi: 10.1039/C6TC00548A.

[70] S. Hu, A. Trinchi, P. Atkin, and I. Cole, "Tunable photoluminescence across the entire visible spectrum from carbon dots excited by white light," *Angew. Chem. Int. Ed. Engl.*, vol. 54, no. 10, pp. 2970–2974, Mar. 2015, doi: 10.1002/ANIE.201411004.

[71] C. T. Chien *et al.*, "Tunable Photoluminescence from Graphene Oxide," *Angew. Chemie Int. Ed.*, vol. 51, no. 27, pp. 6662–6666, Jul. 2012, doi: 10.1002/ANIE.201200474.

[72] D. Li *et al.*, "Near-Infrared Excitation/Emission and Multiphoton-Induced Fluorescence of Carbon Dots," *Adv. Mater.*, vol. 30, no. 13, Mar. 2018, doi: 10.1002/ADMA.201705913.

[73] H. Ding, S. B. Yu, J. S. Wei, and H. M. Xiong, "Full-color light-emitting carbon dots with a surface-state-controlled luminescence mechanism," *ACS Nano*, vol. 10, no. 1, pp. 484–491, Jan. 2016, doi: 10.1021/ACSNANO.5B05406/SUPPL_FILE/NN5B05406_SI_001.PDF.

[74] H. Tetsuka *et al.*, "Optically tunable amino-functionalized graphene quantum dots," *Adv. Mater.*, vol. 24, no. 39, pp. 5333–5338, Oct. 2012, doi: 10.1002/ADMA.201201930.

[75] M. Zheng *et al.*, "Integrating oxaliplatin with highly luminescent carbon dots: an unprecedented theranostic agent for personalized medicine," *Adv. Mater.*, vol. 26, no. 21, pp. 3554–3560, Jun. 2014, doi: 10.1002/ADMA.201306192.

[76] G. Eda *et al.*, "Blue photoluminescence from chemically derived graphene oxide," *Adv. Mater.*, vol. 22, no. 4, pp. 505–509, Jan. 2010, doi: 10.1002/ADMA.200901996.

[77] S. Do *et al.*, "N,S-Induced Electronic States of Carbon Nanodots Toward White Electroluminescence," 2015, doi: 10.1002/adom.201500488.

[78] J. Yu *et al.*, "Luminescence Mechanism of Carbon Dots by Tailoring Functional Groups for Sensing Fe3+ Ions," *Nanomater. 2018, Vol. 8, Page 233*, vol. 8, no. 4, p. 233, Apr. 2018, doi: 10.3390/NANO8040233.

[79] S. Y. Lim, W. Shen, and Z. Gao, "Carbon quantum dots and their applications," *Chem. Soc. Rev.*, vol. 44, no. 1, pp. 362–381, Dec. 2014, doi: 10.1039/C4CS00269E.

[80] H. Ding, X. H. Li, X. B. Chen, J. S. Wei, X. B. Li, and H. M. Xiong, "Surface states of carbon dots and their influences on luminescence," *J. Appl. Phys.*, vol. 127, no. 23, 2020, doi: 10.1063/1.5143819.

[81] S. Zhu, Y. Song, J. Shao, X. Zhao, and B. Yang, "Non-Conjugated Polymer Dots with Crosslink-Enhanced Emission in the Absence of Fluorophore Units," *Angew. Chem. Int. Ed. Engl.*, vol. 54, no. 49, pp. 14626–14637, Dec. 2015, doi: 10.1002/ANIE.201504951.

[82] S. G. Liu *et al.*, "Water-Soluble Nonconjugated Polymer Nanoparticles with Strong Fluorescence Emission for Selective and Sensitive Detection of Nitro-Explosive Picric Acid in Aqueous Medium," *ACS Appl. Mater. Interfaces*, vol. 8, no. 33, pp. 21700–21709, Aug. 2016, doi: 10.1021/ACSAMI.6B07407/SUPPL_FILE/AM6B07407_SI_001.PDF.

[83] F. Ehrat *et al.*, "Tracking the Source of Carbon Dot Photoluminescence: Aromatic Domains versus Molecular Fluorophores.," *Nano Lett.*, vol. 17, no. 12, pp. 7710–7716, Dec. 2017, doi: 10.1021/ACS.NANOLETT.7B03863.

[84] S. Lu *et al.*, "PH-Dependent Synthesis of Novel Structure-Controllable Polymer-Carbon NanoDots with High Acidophilic Luminescence and Super Carbon Dots Assembly for White Light-Emitting Diodes," *ACS Appl. Mater. Interfaces*, vol. 8, no. 6, pp. 4062–4068, Feb. 2016, doi: 10.1021/ACSAMI.5B11579/ASSET/IMAGES/LARGE/AM-2015-11579J_0006.JPEG.

[85] Y. Chong *et al.*, "Crossover between Anti- and Pro-oxidant Activities of Graphene Quantum Dots in the Absence or Presence of Light," *ACS Nano*, vol. 10, no. 9, pp. 8690–8699, 2016, doi: 10.1021/acsnano.6b04061.

[86] V. Ruiz, L. Yate, I. García, G. Cabanero, and H. J. Grande, "Tuning the antioxidant activity of graphene quantum dots: Protective nanomaterials against dye decoloration," *Carbon N. Y.*, vol. 116, pp. 366–374, 2017, doi: 10.1016/j.carbon.2017.01.090.

[87] Y. Qiu *et al.*, "Antioxidant chemistry of graphene-based materials and its role in oxidation protection technology," *Nanoscale*, vol. 6, no. 20, pp. 11744–11755, Sep. 2014, doi: 10.1039/C4NR03275F.

[88] P. Das, S. Ganguly, S. Margel, and A. Gedanken, "Immobilization of Heteroatom-Doped Carbon Dots onto Nonpolar Plastics for Antifogging, Antioxidant, and Food Monitoring Applications," *Langmuir*, vol. 37, no. 11, pp. 3508–3520, 2021, doi: 10.1021/acs.langmuir.1c00471.

[89] J. S. Wright, E. R. Johnson, and G. A. DiLabio, "Predicting the activity of phenolic antioxidants: theoretical method, analysis of substituent effects, and application to major families of antioxidants," *J. Am. Chem. Soc.*, vol. 123, no. 6, pp. 1173–1183, Feb. 2001, doi: 10.1021/JA002455U.

[90] Y. Nosaka and A. Y. Nosaka, "Generation and Detection of Reactive Oxygen Species in Photocatalysis," *Chem. Rev.*, vol. 117, no. 17, pp. 11302–11336, Sep. 2017, doi: 10.1021/ACS.CHEMREV.7B00161.

[91] K. J. Mintz *et al.*, "A deep investigation into the structure of carbon dots," *Carbon N. Y.*, vol. 173, pp. 433–447, 2021, doi: 10.1016/j.carbon.2020.11.017.

[92] S. Pidkova and P. A. Tagliaferro, "Politecnico di Torino Department of Applied Science and Technology Synthesis and characterization of bismuth oxide based and c-dots hybrid materials for teragnostic applications Supervisor : Contents," no. October, 2021.